DOA Estimation of Temporally and Spatially Correlated Narrowband Noncircular Sources in Spatially Correlated White Noise

Sonia Ben Hassen, Faouzi Bellili, Abdelaziz Samet, *Member, IEEE*, and Sofiène Affes, *Senior Member, IEEE*

***Abstract*—The main contribution of our work consists in developing for the first time a method of estimating the direction of arrival (DOA) parameters assuming noncircular and temporally and spatially correlated signals. This new approach, based on a significant enhancement of the two-sided instrumental variable signal subspace fitting (IV-SSF) method, outperforms its classical version in terms of lower bias and error variance. Moreover, it will be shown that our new method is statistically more efficient than the MODE method especially in the case of partly and fully coherent signals where only the extended and the classical two-sided IV-SSF methods are applicable. We also derive an explicit expression for the stochastic Cramér–Rao bound (CRB) of the DOA estimates from temporally and spatially correlated signals generated from noncircular sources. The new CRB is compared to those of circular temporally correlated and noncircular independent and identically distributed signals to show that the CRB obtained assuming both noncircular sources and temporally correlated signals is lower than the CRBs derived considering only one of these two assumptions. This illustrates the potential gain that both noncircularity and temporal correlation provide when considered together. It will also be proven that the difference between the three CRBs increases with the number of snapshots. However, as the signal-to-noise ratio (SNR) increases, the CRBs merge together and decrease linearly. Moreover, at low SNR values it will be shown that temporal correlation is more informative about the unknown DOA parameters than noncircularity. Finally, the CRB derived assuming noncircular and temporally correlated signals depends on the noncircularity rate, the circularity phase separation, and the DOA separation.**

***Index Terms*—DOA estimation, noncircularity of the signals, spatial correlation, stochastic Cramér–Rao lower bound (CRLB), temporal correlation.**

I. Introduction

DIRECTION of arrival (DOA) estimation for multiple plane waves impinging on an arbitrary array of sensors has received a significant amount of attention over the last several decades. It has typically played an important role in array signal processing areas such as modern wireless communication systems, radar, sonar, audio/speech processing systems and radio astronomy. In this context, many DOA estimators have been extensively studied assuming different data models. Indeed, a number of high resolution DOA estimation algorithms have been developed assuming the signals to be independent and identically distributed (iid) and generated from circular sources. The well-known estimators derived in this case are the deterministic (or conditional) and the unconditional maximum-likelihood (ML) estimators [1]. However, the ML estimator is computationally quite expensive due to the required multivariate nonlinear maximization. Therefore, the researchers have derived the so-called eigenstructure or signal subspace methods such as the MUltiple SIgnal Classification (MUSIC) estimator [2], [3] and the Estimation of Signal parameters via Rotational Invariance Technique (ESPRIT) estimator [4] which represent more computationally attractive methods for DOA estimation. Despite their relatively reduced computational cost, these two techniques were proved to be statistically less accurate than the ML estimator. The Method Of DOA Estimation (MODE) technique, a new method that advocates a compromise between the good performance of the ML method and the computational simplicity of MUSIC was later proposed in [5]. However, this method was shown to be statistically inefficient in the case of coherent sources. Furthermore, authors have proposed in [6] some signal subspace fitting (SSF) methods. In fact, the MD-MUSIC an alternative multidimensional array processing technique based on subspace fitting was derived as an extension of the one-dimensional MUSIC algorithm. This estimator was proved to be performed by an optimal multidimensional subspace fitting based technique referred as the weighted subspace fitting (WSF) method. This technique was shown to be asymptotically identical to the MODE estimator when the sources are non coherent. However, for coherent sources only WSF is efficient [7]. Yet, in the last few decades, there has been interest in developing other algorithms to improve DOA estimation capability. These algorithms consider more realistic assumptions in the data models. In fact, the decoupled maximum-likelihood (DEML) angle estimator [8] assumes that the waveforms of the incident signals are known but the amplitudes are unknown and also supposes the noise to be unknown and arbitrarily spatially colored. Furthermore, some other contributions [9]–[11] have addressed the problem of DOA estimation in unknown noise environments based on various assumptions regarding the noise.

Manuscript received September 30, 2010; revised March 03, 2011; accepted April 28, 2011. Date of publication May 27, 2011; date of current version August 10, 2011. The associate editor coordinating the review of this manuscript and approving it for publication was Prof. Alfred Hanssen. This work was supported by a Canada Research Chair in Wireless Communications and a Discovery Accelerator Supplement from NSERC.

The authors are with the INRS-EMT, Montreal, QC H5A 1K6, Canada (e-mail: hassen@emt.inrs.ca; bellili@emt.inrs.ca; abdelaziz.samet@ept.rnu.tn; affes@emt.inrs.ca).

Color versions of one or more of the figures in this paper are available online at http://ieeexplore.ieee.org.

Digital Object Identifier 10.1109/TSP.2011.2157499

Despite their efficiency, all the aforementioned estimators present some practical limitations. In fact, they are mainly developed assuming the snapshots to be iid or uncorrelated in time. This iid assumption presents a challenging limitation on the applicability of the results in the real world and results in some practical difficulties. Therefore, efforts have been directed to considering more realistic models assuming the signals to be temporally correlated. In this context, a novel instrumental variable (IV) approach to the sensor array problem is proposed in [12]. This IV technique that assumes the signals to be temporally correlated and circular Gaussian distributed does not require any knowledge of the noise covariance matrix but its uncorrelatedness in time. Although the IV method was proved to be computationally much less expensive than the eigendecomposition or ML-based techniques, it was shown to give inaccurate estimates in difficult scenarios involving highly correlated and/or closely spaced signals. Therefore, authors have proposed in [13] a new IV method that combines the ideas of SSF and IV. This combination results in a more computationally complex method than the one presented in [12]. However, the new method was proved to be statistically greatly accurate as compared to the previous technique especially in the case of highly and fully correlated signals.

Yet, noncircular complex signals, for example binary phase shift keying (BPSK) and offset-quadrature-phase-shift-keying (OQPSK) modulated signals, are frequently encountered in digital communications. Therefore, more recently, there has been a considerable interest in deriving new algorithms that exploit the unconjugated spatial covariance matrix for noncircular signals [14], [15]. More recently, Haddadi, Nayebi, and Aref proposed in [16] a new algorithm that presents an improved version of the method developed in [13], but still for circular signals. To the best of our knowledge, however, no contributions have dealt yet with the problem of estimating the DOA assuming the signals to be temporally and spatially correlated and also generated from noncircular sources. Therefore, the aim of this work is to tackle DOA estimation in the case of both temporal correlation and noncircularity of the signals.

In this paper, we propose an algorithm that extends the recent method developed in [16] assuming circular signals in the case of noncircular signals. We also conduct a complete study of the statistical properties of the new algorithm. Furthermore, we derive for the first time an explicit expression for the CRB of the DOA estimates from temporally and possibly spatially correlated signals generated from noncircular sources.

This paper is organized as follows. In Section II, we introduce the system model that will be used throughout the article and we define the problem in terms of notation and assumptions. In Section III, we formulate the proposed algorithm and discuss its statistical properties. In Section IV, an explicit expression for the DOA CRB assuming temporally and spatially correlated signals generated from noncircular sources will be derived. In Section V, the proposed method is compared to that in [15] and to the corresponding CRB through computer simulations.

Throughout this paper, matrices and vectors are represented by bold upper case and bold lower case characters, respectively. Vectors are, by default, in column orientation. Moreover, we consider the following notations.

Notations:

$(.)^*$	Conjugate.
$(.)^T$	Transpose.
$(.)^H$	Conjugate transpose.
$\mathrm{tr}(.)$	Trace.
$\|.\|_{\mathrm{Fro}}$	Frobenius norm.
$\Re\{.\}$	Real part operator.
$\Im\{.\}$	Imaginary part operator.
$\mathrm{E}\{.\}$	Expectation operator.
$\mathrm{eig}(.)$	Eigenvalues of a matrix.
$\otimes$	Kronecker operator.
$\odot$	Hadamard–Schur product operator.
$\boldsymbol{I}_p$	$(p \times p)$ identity matrix.
$\boldsymbol{0}_{p\times q}$	$(p \times q)$ null matrix.
$\boldsymbol{A\theta} = \boldsymbol{A}$	$= [\boldsymbol{a}(\theta_1), \ldots, \boldsymbol{a}(\theta_K)]$; steering matrix.
$\boldsymbol{a}(\theta_i)$	Array steering vector parameterized by θ_i.
$\boldsymbol{D}$	$= [\boldsymbol{d}_1, \ldots, \boldsymbol{d}_K]\,; \boldsymbol{d}_i = \frac{\partial \boldsymbol{a}(\theta_i)}{\partial \theta_i}$.
$\boldsymbol{D}_i$	$= \frac{\partial \boldsymbol{A}(\boldsymbol{\theta})}{\partial \theta_i} = [\boldsymbol{0}_{L\times 1}, \ldots, \boldsymbol{d}_i, \ldots, \boldsymbol{0}_{L\times 1}]$.
$\boldsymbol{\Pi}^{\perp}_{\boldsymbol{A}}(\boldsymbol{\theta}) = \boldsymbol{\Pi}^{\perp}_{\boldsymbol{A}}$	$= \boldsymbol{I}_L - \boldsymbol{A}\left(\boldsymbol{A}^H\boldsymbol{A}\right)^{-1}\boldsymbol{A}^H(\theta)$; orthogonal projection onto the null space of $\boldsymbol{A}$.
$\boldsymbol{\mathcal{P}}^{ik}$	ikth block of block matrix $\boldsymbol{\mathcal{P}}$.
$\boldsymbol{\mathcal{P}}'^{ik}$	ikth block of block matrix $\boldsymbol{\mathcal{P}}'$.
$\mathrm{Block}_{ik}[\boldsymbol{\mathcal{P}}^{ik}]$	Block matrix with blocks $\boldsymbol{\mathcal{P}}^{ik}$.
$\mathrm{Block}_{ik}[\boldsymbol{\mathcal{P}}'^{ik}]$	Block matrix with blocks $\boldsymbol{\mathcal{P}}'^{ik}$.
$\boldsymbol{A} \geq \boldsymbol{B}$	$\boldsymbol{A} - \boldsymbol{B}$ is positive semi-definite matrix.
$\mathrm{Btr}_K(\boldsymbol{\mathcal{P}})$	$= \sum_i \boldsymbol{\mathcal{P}}^{ii}_{K\times K}$; block trace.

II. System Model

Consider an array of L sensors receiving the signals emitted by K narrowband sources with directions $\boldsymbol{\theta} = [\theta_1, \ldots, \theta_K]$. Then, the received data can be modeled as a complex signal as follows:

$$\boldsymbol{y}_{L\times 1}(t) = \boldsymbol{A}_{L\times K}\,\boldsymbol{x}_{K\times 1}(t) + \boldsymbol{w}_{L\times 1}(t),\ t = 1, 2, \ldots, N \quad (1)$$

where N represents the total number of received samples in the observation window. At time index t, $\boldsymbol{x}(t)$ is the sources' transmitted signals and $\boldsymbol{w}(t)$ is the sensors noise vector.

Stacking the received data over the whole observation window in a matrix $\boldsymbol{Y}$, (1) can be written in a matrix form as follows:

$$\boldsymbol{Y} = \boldsymbol{A}\,\boldsymbol{X} + \boldsymbol{W} \quad (2)$$

where $\boldsymbol{Y} = [\boldsymbol{y}(1), \ldots, \boldsymbol{y}(N)]$ represents the data samples, $\boldsymbol{X} = [\boldsymbol{x}(1), \ldots, \boldsymbol{x}(N)]$ is the signal sequence and $\boldsymbol{W} = [\boldsymbol{w}(1), \ldots, \boldsymbol{w}(N)]$ is the noise sequence.

The transmitted signals $\boldsymbol{x}(t)$ are assumed to be generated from noncircular sources. This means that $\mathrm{E}\{\boldsymbol{x}(t)\boldsymbol{x}^T(t)\} \neq \boldsymbol{0}$ contrarily to circular signals. Otherwise, the transmitted signals $\{\boldsymbol{x}(t)\}_{t=1,2,\ldots,N}$ are supposed to be zero-mean complex noncircular, temporally and possibly spatially correlated with conjugated and unconjugated covariance matrices $\boldsymbol{\mathcal{P}}_{NK\times NK}$ and $\boldsymbol{\mathcal{P}}'_{NK\times NK}$, respectively, as follows:

$$\boldsymbol{\mathcal{P}}_{NK\times NK} = \mathrm{Block}_{ik}[\boldsymbol{\mathcal{P}}^{ik}_{K\times K}] \tag{3}$$

$$\boldsymbol{\mathcal{P}}'_{NK\times NK} = \mathrm{Block}_{ik}[\boldsymbol{\mathcal{P}}'^{ik}_{K\times K}]. \tag{4}$$

The ikth block of the block matrix $\boldsymbol{\mathcal{P}}$ $\boldsymbol{\mathcal{P}}^{ik}$ represents the first space-time covariance matrix of the signals and is defined as

$$\boldsymbol{\mathcal{P}}^{ik} = \boldsymbol{P}_{ik} = \mathrm{E}\{\boldsymbol{x}(i)\boldsymbol{x}^H(k)\}. \tag{5}$$

Moreover, the ikth block of the block matrix $\boldsymbol{\mathcal{P}}'$, $\boldsymbol{\mathcal{P}}'^{ik}$, represents the second non-singular covariance matrix of the signals and is defined as

$$\boldsymbol{\mathcal{P}}'^{ik} = \boldsymbol{P}'_{ik} = \mathrm{E}\{\boldsymbol{x}(i)\boldsymbol{x}^T(k)\}. \tag{6}$$

The noise is assumed to be zero-mean Gaussian complex circular, possibly spatially correlated and temporally uncorrelated with conjugated covariance matrix

$$\boldsymbol{\mathcal{C}} = \boldsymbol{I}_N \otimes \boldsymbol{C} \tag{7}$$

where $\boldsymbol{C}$ represents the noise covariance matrix defined as follows:

$$\boldsymbol{C} = \mathrm{E}\{\boldsymbol{w}(t)\boldsymbol{w}^H(t)\}. \tag{8}$$

Consequently, the received signals are zero-mean complex noncircular, temporally and possibly spatially correlated with conjugated and unconjugated covariance matrices $\boldsymbol{\mathcal{R}}_{NL\times NL}$ and $\boldsymbol{\mathcal{R}}'_{NL\times NL}$, respectively, as follows:

$$\boldsymbol{\mathcal{R}}_{NL\times NL} = \boldsymbol{\mathcal{A}}\boldsymbol{\mathcal{P}}\boldsymbol{\mathcal{A}}^H + \boldsymbol{\mathcal{C}} \tag{9}$$

$$\boldsymbol{\mathcal{R}}'_{NL\times NL} = \boldsymbol{\mathcal{A}}\boldsymbol{\mathcal{P}}\boldsymbol{\mathcal{A}}^T \tag{10}$$

where

$$\boldsymbol{\mathcal{A}} = \boldsymbol{I}_N \otimes \boldsymbol{A}. \tag{11}$$

In this paper, we consider the same assumptions A1), A2), and A3) recently introduced in [13] as follows.

A1) It is assumed that $K < L$ and that for any set of distinct DOA parameters $\theta_1, \ldots, \theta_K$, the vectors $\{\boldsymbol{a}(\theta_1), \ldots, \boldsymbol{a}(\theta_K)\}$ are linearly independent. Furthermore, $\boldsymbol{a}(\theta)$ is assumed to be differentiable with respect to θ and the true parameter vector $\boldsymbol{\theta}_0$ is an inner point of the set of parameter vectors of interest.

A2) The transmitted signals $\{\boldsymbol{x}(t)\}_{t=1,2,\ldots,N}$ are assumed to be independent from the noise components $\{\boldsymbol{w}(t)\}_{t=1,2,\ldots,N}$.

A3) Define the first cross-covariance matrix of the transmitted signals at time lag k as follows:

$$\boldsymbol{P}_k = \mathrm{E}\{\boldsymbol{x}(t-k)\boldsymbol{x}^H(t \tag{12}$$

and introduce the matrix of stacked first cross-covariances as follows:

$$\boldsymbol{\mathcal{J}} = \left[\, \boldsymbol{P}_{-\frac{M}{2}}, \ldots, \boldsymbol{P}_{-1},\ \boldsymbol{P}_1, \ldots, \boldsymbol{P}_{\frac{M}{2}} \,\right]^T. \tag{13}$$

The signals are assumed to exhibit a "sufficient" temporal correlation so that no column of $\boldsymbol{\mathcal{J}}$ is identically zero and so that the rank of $\boldsymbol{\mathcal{J}}$, denoted μ, satisfies $\mu > 2K - L$.

III. Extension of the IV-SSF Method to Noncircular Signals

In the case of an unknown noise spatial covariance matrix, the IV-SSF method for DOA estimation in the case of circular sources has been first introduced in [13]. This method is based on an instrumental variable vector containing only the M previous data samples of the received signal $\boldsymbol{y}(t)$ as follows:

$$\boldsymbol{\phi}(t) = [\, \boldsymbol{y}(t-1), \ldots, \boldsymbol{y}(t-M) \,]^T$$

where M is an integer, larger than 1 determining the degree of complexity and hence the performance of the method. More recently, the authors of [16] proposed a variation of this method by defining a two-sided instrumental variable vector containing M data samples collected before and after the current sample $\boldsymbol{y}(t)$ as follows:

$$\boldsymbol{\phi}(t) = [\, \boldsymbol{y}(t+\tfrac{M}{2}), \ldots, \boldsymbol{y}(t+1), \boldsymbol{y}(t-1), \ldots, \boldsymbol{y}(t-\tfrac{M}{2}) \,]^T \tag{14}$$

where M is an even integer larger than 2. This new version was proved to outperform the previous one in terms of lower bias and error variance. In this paper, we propose an enhanced version of the classical instrumental variable method that generalizes its new application to noncircular sources based on its recent variation extended in [16] to time correlated sources.

A. Extended IV-SSF Method

Let us first consider the two-sided instrumental variables vector defined in (14). Next, in order to take advantage of the signal noncircularity, we define the extended two-sided instrumental variables vector as follows:

$$\tilde{\boldsymbol{\phi}}(t) = \left[\, \boldsymbol{\phi}(t),\ \boldsymbol{\phi}^*(t) \,\right]^T. \tag{15}$$

Then, we introduce the first cross-covariance matrix of the transmitted signals at time lag k as defined in (12) and the second

cross-covariance matrix of the transmitted signals at time lag k as follows:

$$\boldsymbol{P}'_k = \mathrm{E}\{\boldsymbol{x}(t-k)\boldsymbol{x}^T(t)\}. \tag{16}$$

The extended cross-covariance of the received data and the corresponding instrumental variable is

$$\tilde{\boldsymbol{\Sigma}} = \mathrm{E}\left\{\tilde{\boldsymbol{\phi}}(t)\tilde{\boldsymbol{y}}^H(t)\right\} \tag{17}$$

where $\tilde{\boldsymbol{y}}(t)$ is the extended received vector defined as

$$\tilde{\boldsymbol{y}}(t) = \left[\,\boldsymbol{y}(t),\ \boldsymbol{y}^*(t)\,\right]^T. \tag{18}$$

Then, we obtain the following cross-covariance matrix

$$\tilde{\boldsymbol{\Sigma}} = \begin{pmatrix} \boldsymbol{\Sigma} & \boldsymbol{\Sigma}' \\ \boldsymbol{\Sigma}'^* & \boldsymbol{\Sigma}^* \end{pmatrix} \tag{19}$$

where

$$\boldsymbol{\Sigma} = \mathrm{E}\left\{\boldsymbol{\phi}(t)\boldsymbol{y}^H(t)\right\} \tag{20}$$

$$\boldsymbol{\Sigma}' = \mathrm{E}\left\{\boldsymbol{\phi}(t)\boldsymbol{y}^T(t)\right\}. \tag{21}$$

Some algebraic manipulations yield the following expressions for $\boldsymbol{\Sigma}$ and $\boldsymbol{\Sigma}'$:

$$\boldsymbol{\Sigma} = \boldsymbol{\mathcal{A}}_M \boldsymbol{\mathcal{J}} \boldsymbol{A}^H \tag{22}$$

$$\boldsymbol{\Sigma}' = \boldsymbol{\mathcal{A}}_M \boldsymbol{\mathcal{J}}' \boldsymbol{A}^T \tag{23}$$

where $\boldsymbol{\mathcal{J}}$ is defined in (13) and $\boldsymbol{\mathcal{A}}_M$ and $\boldsymbol{\mathcal{J}}'$ are defined as follows:

$$\boldsymbol{\mathcal{A}}_M = \boldsymbol{I}_M \otimes \boldsymbol{A} \tag{24}$$

$$\boldsymbol{\mathcal{J}}' = \left[\,\boldsymbol{P}'_{-\frac{M}{2}}, \ldots, \boldsymbol{P}'_{-1},\ \boldsymbol{P}'_1, \ldots, \boldsymbol{P}'_{\frac{M}{2}}\,\right]^T \tag{25}$$

with $\{\boldsymbol{P}'_k\}_{k=-\frac{M}{2}}^{\frac{M}{2}}$ being defined in (16). Consequently, the extended cross-covariance matrix of the received data and the corresponding instrumental variable can be easily shown to be

$$\tilde{\boldsymbol{\Sigma}} = \tilde{\boldsymbol{\mathcal{A}}}_M \tilde{\boldsymbol{\mathcal{J}}} \tilde{\boldsymbol{A}}^H \tag{26}$$

where

$$\tilde{\boldsymbol{\mathcal{A}}}_M = \begin{pmatrix} \boldsymbol{\mathcal{A}}_M & \boldsymbol{0}_{LM\times KM} \\ \boldsymbol{0}_{LM\times KM} & \boldsymbol{\mathcal{A}}_M{}^* \end{pmatrix}$$

$$\tilde{\boldsymbol{\mathcal{J}}} = \begin{pmatrix} \boldsymbol{\mathcal{J}} & \boldsymbol{\mathcal{J}}' \\ \boldsymbol{\mathcal{J}}'^* & \boldsymbol{\mathcal{J}}^* \end{pmatrix}$$

$$\tilde{\boldsymbol{A}} = \begin{pmatrix} \boldsymbol{A}^H & \boldsymbol{0}_{K\times L} \\ \boldsymbol{0}_{K\times L} & \boldsymbol{A}^T \end{pmatrix}.$$

We also define the extended instrumental variable covariance matrix as follows:

$$\tilde{\boldsymbol{\Phi}} = \mathrm{E}\left\{\tilde{\boldsymbol{\phi}}(t)\tilde{\boldsymbol{\phi}}^H(t)\right\} = \begin{pmatrix} \boldsymbol{\Phi} & \boldsymbol{\Phi}' \\ \boldsymbol{\Phi}'^* & \boldsymbol{\Phi}^* \end{pmatrix} \tag{27}$$

where

$$\boldsymbol{\Phi} = \mathrm{E}\left\{\boldsymbol{\phi}(t)\boldsymbol{\phi}^H(t)\right\} \tag{28}$$

$$\boldsymbol{\Phi}' = \mathrm{E}\left\{\boldsymbol{\phi}(t)\boldsymbol{\phi}^T(t)\right\}. \tag{29}$$

To determine the sample estimates of $\tilde{\boldsymbol{\Sigma}}$ and $\tilde{\boldsymbol{\Phi}}$ denoted as $\hat{\tilde{\boldsymbol{\Sigma}}}$ and $\hat{\tilde{\boldsymbol{\Phi}}}$, respectively, we consider the two following conditions:

$$1 \le t + \frac{M}{2} \le N$$

$$1 \le t - \frac{M}{2} \le N.$$

Then, we have

$$1 + \frac{M}{2} \le t \le N - \frac{M}{2}.$$

Consequently, the sample estimates $\hat{\tilde{\boldsymbol{\Sigma}}}$ and $\hat{\tilde{\boldsymbol{\Phi}}}$ are defined as follows:

$$\hat{\tilde{\boldsymbol{\Sigma}}} = \frac{1}{N-M} \sum_{t=\frac{M}{2}+1}^{N-\frac{M}{2}} \tilde{\boldsymbol{\phi}}(t)\tilde{\boldsymbol{y}}^H(t) \tag{30}$$

$$\hat{\tilde{\boldsymbol{\Phi}}} = \frac{1}{N-M} \sum_{t=\frac{M}{2}+1}^{N-\frac{M}{2}} \tilde{\boldsymbol{\phi}}(t)\tilde{\boldsymbol{\phi}}^H(t). \tag{31}$$

Consider here the Assumption A3). We denote μ' the rank of $\tilde{\boldsymbol{\mathcal{J}}}$. Then, we have $\mu \le \mu' \le 2\mu$. Moreover, we consider the assumption $A1$. The matrix $\boldsymbol{A}$ has a full rank. Therefore, the matrices $\boldsymbol{\mathcal{A}}_M$ and $\tilde{\boldsymbol{\mathcal{A}}}_M$ have full ranks. Consequently, we have $\mathrm{rank}(\tilde{\boldsymbol{\Sigma}}) = \mathrm{rank}(\tilde{\boldsymbol{\mathcal{J}}}) = \mu'$. The singular value decomposition (SVD) of the matrix $\tilde{\boldsymbol{\Phi}}^{-\frac{1}{2}}\tilde{\boldsymbol{\Sigma}}$ yields the following result:

$$\tilde{\boldsymbol{\Phi}}^{-\frac{1}{2}}\tilde{\boldsymbol{\Sigma}} = \tilde{\boldsymbol{U}}_s \tilde{\boldsymbol{\Delta}}_s \tilde{\boldsymbol{V}}_s^H \tag{32}$$

where

$$\tilde{\boldsymbol{\Delta}}_s = \sqrt{\mathrm{eig}\left(\tilde{\boldsymbol{\Phi}}^{-\frac{1}{2}}\tilde{\boldsymbol{\Sigma}}\tilde{\boldsymbol{\Sigma}}^H\tilde{\boldsymbol{\Phi}}^{-\frac{1}{2}}\right)}. \tag{33}$$

Then, $\mathrm{rank}(\tilde{\boldsymbol{\Delta}}_s) = \mathrm{rank}(\tilde{\boldsymbol{\Sigma}}) = \mu'$. From (26) and (32), we show that the range space of $\tilde{\boldsymbol{V}}_s$ is contained in the one of $\tilde{\boldsymbol{A}}$. Consequently, there exists a full rank $2K \times \mu'$ matrix $\boldsymbol{T}$ such that

$$\tilde{\boldsymbol{V}}_s = \tilde{\boldsymbol{A}}(\boldsymbol{\theta})\boldsymbol{T}. \tag{34}$$

In the same way, we consider the sample estimates $\hat{\tilde{\boldsymbol{\Sigma}}}$ and $\hat{\tilde{\boldsymbol{\Phi}}}$ already defined in (30) and (31), respectively. The SVD of the matrix $\hat{\tilde{\boldsymbol{\Phi}}}^{-\frac{1}{2}}\hat{\tilde{\boldsymbol{\Sigma}}}$ yields the following result:

$$\hat{\tilde{\boldsymbol{\Phi}}}^{-\frac{1}{2}}\hat{\tilde{\boldsymbol{\Sigma}}} = \hat{\tilde{\boldsymbol{U}}}_s \hat{\tilde{\boldsymbol{\Delta}}}_s \hat{\tilde{\boldsymbol{V}}}_s^H + \hat{\tilde{\boldsymbol{U}}}_n \hat{\tilde{\boldsymbol{\Delta}}}_n \hat{\tilde{\boldsymbol{V}}}_n^H \tag{35}$$

where the matrix $\hat{\tilde{\boldsymbol{\Delta}}}_s$ contains the μ' largest singular values. Then, we have, similarly to the result obtained in [13], the following separable least-squares problem:

$$\left\{\hat{\boldsymbol{\theta}}, \hat{\boldsymbol{T}}\right\} = \arg\min_{\boldsymbol{\theta},\boldsymbol{T}} \left\| \hat{\tilde{\boldsymbol{C}}}^{-\frac{1}{2}} (\hat{\tilde{\boldsymbol{V}}}_s \hat{\tilde{\boldsymbol{\Delta}}}_s - \tilde{\boldsymbol{A}}\boldsymbol{T}) \right\|_{\mathrm{Fro}}^2 \tag{36}$$

where

$$\tilde{\boldsymbol{C}} = \begin{pmatrix} \boldsymbol{C} & \boldsymbol{0}_{L\times L} \\ \boldsymbol{0}_{L\times L} & \boldsymbol{C}^* \end{pmatrix}. \tag{37}$$

We minimize the term $\left\| \hat{\hat{\boldsymbol{C}}}^{-\frac{1}{2}} (\hat{\hat{\boldsymbol{V}}}_s \hat{\hat{\boldsymbol{\Delta}}}_s - \tilde{\boldsymbol{A}}\boldsymbol{T}) \right\|_{\text{Fro}}^2$ with respect to $\boldsymbol{T}$ and use some properties of the derivative of the trace. We hence obtain the following expression for $\hat{\boldsymbol{T}}$:

$$\hat{\boldsymbol{T}} = \left(\tilde{\boldsymbol{A}}^H \hat{\hat{\boldsymbol{C}}}^{-1} \tilde{\boldsymbol{A}} \right)^{-1} \tilde{\boldsymbol{A}}^H \hat{\hat{\boldsymbol{C}}}^{-1} \hat{\hat{\boldsymbol{V}}}_s \hat{\hat{\boldsymbol{\Delta}}}_s. \tag{38}$$

Inserting (38) in (36) and some algebraic manipulations yield the following criterion function:

$$\hat{\boldsymbol{\theta}} = \arg\min_{\boldsymbol{\theta}} V(\boldsymbol{\theta}) \tag{39}$$

where

$$V(\boldsymbol{\theta}) = \operatorname{tr}\left(\hat{\hat{\boldsymbol{\Pi}}}_0^{\perp} \hat{\hat{\boldsymbol{C}}}^{-\frac{1}{2}} \hat{\hat{\boldsymbol{V}}}_s \hat{\hat{\boldsymbol{\Delta}}}_s^2 \hat{\hat{\boldsymbol{V}}}_s^H \hat{\hat{\boldsymbol{C}}}^{-\frac{1}{2}} \right) \tag{40}$$

$$\hat{\hat{\boldsymbol{\Pi}}}_0^{\perp} = \boldsymbol{\Pi}^{\perp}_{\hat{\hat{\boldsymbol{C}}}^{-\frac{1}{2}} \tilde{\boldsymbol{A}}}. \tag{41}$$

This criterion is statistically equivalent to the following one

$$\hat{\boldsymbol{\theta}} = \arg\min_{\boldsymbol{\theta}} \operatorname{tr}\left(\hat{\hat{\boldsymbol{\Pi}}}^{\perp} \hat{\hat{\boldsymbol{R}}}_0^{-\frac{1}{2}} \hat{\hat{\boldsymbol{V}}}_s \hat{\hat{\boldsymbol{\Delta}}}_s^2 \hat{\hat{\boldsymbol{V}}}_s^H \hat{\hat{\boldsymbol{R}}}_0^{-\frac{1}{2}} \right), \tag{42}$$

where

$$\hat{\hat{\boldsymbol{\Pi}}}^{\perp} = \boldsymbol{\Pi}^{\perp}_{\hat{\hat{\boldsymbol{R}}}_0^{-\frac{1}{2}} \tilde{\boldsymbol{A}}}. \tag{43}$$

$\hat{\hat{\boldsymbol{R}}}_0$ represents an estimate of $\tilde{\boldsymbol{R}}_0 = \mathrm{E}\{\tilde{\boldsymbol{y}}(t)\tilde{\boldsymbol{y}}^H(t)\}$. Then, the estimates of the DOAs using our extended version of the IV-SSF method are obtained in different steps. First, we choose an even integer $M \geq 2$, and we compute the sample estimates $\hat{\hat{\boldsymbol{\Sigma}}}$ and $\hat{\hat{\boldsymbol{\Phi}}}$ defined in (30) and (31), respectively. Second, we perform the SVD of the matrix $\hat{\hat{\boldsymbol{\Phi}}}^{-\frac{1}{2}} \hat{\hat{\boldsymbol{\Sigma}}}$, and we extract the corresponding dominant right singular vectors in the matrix $\hat{\hat{\boldsymbol{V}}}_s$ and the associated singular values in the matrix $\hat{\hat{\boldsymbol{\Delta}}}_s$. We later extract $\hat{\boldsymbol{R}}_0$ as one of the $L \times L$ diagonal blocks of the block matrix $(\hat{\hat{\boldsymbol{\Phi}}})_{1:ML,1:ML}$ and $\hat{\boldsymbol{R}}_0'$ as one of the $L \times L$ diagonal blocks of the block matrix $(\hat{\hat{\boldsymbol{\Phi}}})_{1:ML,ML+1:2ML}$ and we obtain $\hat{\hat{\boldsymbol{R}}}_0$ as follows:

$$\hat{\hat{\boldsymbol{R}}}_0 = \begin{pmatrix} \hat{\boldsymbol{R}}_0 & \hat{\boldsymbol{R}}_0' \\ \hat{\boldsymbol{R}}_0'^* & \hat{\boldsymbol{R}}_0^* \end{pmatrix}. \tag{44}$$

Finally, the DOAs are estimated as the locations of the smallest minima of the function

$$g_N(\theta) = \operatorname{tr}\left(\hat{\hat{\boldsymbol{\Pi}}}_N^{\perp}(\theta) \hat{\hat{\boldsymbol{R}}}_0^{-\frac{1}{2}} \hat{\hat{\boldsymbol{V}}}_s \hat{\hat{\boldsymbol{\Delta}}}_s^2 \hat{\hat{\boldsymbol{V}}}_s^H \hat{\hat{\boldsymbol{R}}}_0^{-\frac{1}{2}} \right),$$

where

$$\hat{\hat{\boldsymbol{\Pi}}}_N^{\perp}(\theta) = \boldsymbol{\Pi}^{\perp}_{\hat{\hat{\boldsymbol{R}}}_0^{-\frac{1}{2}} \bar{\boldsymbol{A}}(\theta)},$$

where $\bar{\boldsymbol{A}}(\theta)$ is the steering matrix

$$\bar{\boldsymbol{A}}(\theta) = \begin{pmatrix} \boldsymbol{a}(\theta) & \boldsymbol{0}_{L\times 1} \\ \boldsymbol{0}_{L\times 1} & \boldsymbol{a}^*(\theta) \end{pmatrix}.$$

Note here that comparing the extended two-sided IV-SSF algorithm with the classical two-sided IV-SSF one developed in [16], we see clearly that the extension of the circular method to noncircular signals results in a more computationally complex method.

B. Statistical Properties

Similarly to [13], the minimizer of (39) converges with probability one (w.p.1) to the true parameter vector $\boldsymbol{\theta}_0$. Moreover, we denote $\tilde{\boldsymbol{\theta}} = \hat{\boldsymbol{\theta}} - \boldsymbol{\theta}_0$ the difference between the estimated parameter vector and the true parameter vector. Then, from standard statistical theory, the asymptotic distribution of $\tilde{\boldsymbol{\theta}}$ is Gaussian with zero mean and covariance matrix

$$\boldsymbol{C}_v = \boldsymbol{H}^{-1}\boldsymbol{Q}\boldsymbol{H}^{-1} \tag{45}$$

where

$$\boldsymbol{H} = \lim_{N \to +\infty} V''(\boldsymbol{\theta}_0), \quad \text{(w.p.1)} \tag{46}$$

$$\boldsymbol{Q} = \lim_{N \to +\infty} N\mathrm{E}\{V'(\boldsymbol{\theta}_0)V'^T(\boldsymbol{\theta}_0)\} \tag{47}$$

with $V'(.)$ and $V''(.)$ denoting the gradient with respect to $\boldsymbol{\theta}$ of $V(.)$ previously defined in (40) and the Hessian matrix, respectively. After some algebraic manipulations (see appendices A and B), we obtain the following expressions for $\boldsymbol{H}$ and $\boldsymbol{Q}$:

$$\boldsymbol{H} = 4\Re\left\{ \left(\boldsymbol{D}^H \boldsymbol{C}^{-\frac{1}{2}} \boldsymbol{\Pi}_0^{\perp} \boldsymbol{C}^{-\frac{1}{2}} \boldsymbol{D} \right) \odot \left((\boldsymbol{\mathcal{J}}^H \boldsymbol{\mathcal{A}}_M^H \boldsymbol{\mathcal{J}}'^T \boldsymbol{\mathcal{A}}_M^T) \tilde{\boldsymbol{\Phi}}^{-1} \begin{pmatrix} \boldsymbol{\mathcal{A}}_M \boldsymbol{\mathcal{J}} \\ \boldsymbol{\mathcal{A}}_M^* \boldsymbol{\mathcal{J}}'^* \end{pmatrix} \right)^T \right\} \tag{48}$$

$$\boldsymbol{Q} = 2\boldsymbol{H}. \tag{49}$$

Consequently, the asymptotic covariance matrix of $\boldsymbol{\theta}$ is given by

$$\boldsymbol{C}_v = \frac{1}{2}\left[\Re\left\{ \left(\boldsymbol{D}^H \boldsymbol{C}^{-\frac{1}{2}} \boldsymbol{\Pi}_0^{\perp} \boldsymbol{C}^{-\frac{1}{2}} \boldsymbol{D} \right) \odot \left((\boldsymbol{\mathcal{J}}^H \boldsymbol{\mathcal{A}}_M^H \boldsymbol{\mathcal{J}}'^T \boldsymbol{\mathcal{A}}_M^T) \tilde{\boldsymbol{\Phi}}^{-1} \begin{pmatrix} \boldsymbol{\mathcal{A}}_M \boldsymbol{\mathcal{J}} \\ \boldsymbol{\mathcal{A}}_M^* \boldsymbol{\mathcal{J}}'^* \end{pmatrix} \right)^T \right\} \right]^{-1}. \tag{50}$$

We note here that in the case of circular sources, we have $\boldsymbol{\mathcal{J}}' = \boldsymbol{0}_{KM\times K}$ and $\boldsymbol{\Phi}' = \boldsymbol{0}_{LM\times LM}$. Therefore, $\tilde{\boldsymbol{\Phi}}$ becomes

$$\tilde{\boldsymbol{\Phi}} = \begin{pmatrix} \boldsymbol{\Phi} & \boldsymbol{0}_{LM\times LM} \\ \boldsymbol{0}_{LM\times LM} & \boldsymbol{\Phi}^* \end{pmatrix}.$$

Consequently, (50) reduces to

$$\boldsymbol{C}_v^{\text{cir}} = \frac{1}{2}\left[\Re\left\{ \left(\boldsymbol{D}^H \boldsymbol{C}^{-\frac{1}{2}} \boldsymbol{\Pi}_0^{\perp} \boldsymbol{C}^{-\frac{1}{2}} \boldsymbol{D} \right) \odot \left(\boldsymbol{\mathcal{J}}^H \boldsymbol{\mathcal{A}}_M^H \boldsymbol{\Phi}^{-1} \boldsymbol{\mathcal{A}}_M \boldsymbol{\mathcal{J}} \right)^T \right\} \right]^{-1},$$

derived in [16] as a special case of our general method.

Now, we denote

$$\begin{aligned}\boldsymbol{B}_1 &= \begin{pmatrix}\boldsymbol{\mathcal{J}}^H\boldsymbol{\mathcal{A}}_M^H & \boldsymbol{\mathcal{J}}'^T\boldsymbol{\mathcal{A}}_M^T\end{pmatrix}\tilde{\boldsymbol{\Phi}}^{-1}\begin{pmatrix}\boldsymbol{\mathcal{A}}_M\boldsymbol{\mathcal{J}}\\ \boldsymbol{\mathcal{A}}_M^*\boldsymbol{\mathcal{J}}'^*\end{pmatrix},\\ \boldsymbol{B}_2 &= \boldsymbol{\mathcal{J}}^H\boldsymbol{\mathcal{A}}_M^H\boldsymbol{\Phi}^{-1}\boldsymbol{\mathcal{A}}_M\boldsymbol{\mathcal{J}},\\ \boldsymbol{B}_3 &= \boldsymbol{D}^H\boldsymbol{C}^{-\frac{1}{2}}\boldsymbol{\Pi}_0^{\perp}\boldsymbol{C}^{-\frac{1}{2}}\boldsymbol{D}.\end{aligned}$$

Applying [1, Lemma A.4] to $\boldsymbol{B}_1$ and $\boldsymbol{B}_2$, we obtain $\boldsymbol{B}_1 \geq \boldsymbol{B}_2$. This inequality applies to the transpose of these matrices. Then, we have $\boldsymbol{B}_1^T - \boldsymbol{B}_2^T \geq \boldsymbol{0}$. Moreover, we have $\boldsymbol{B}_3 \geq \boldsymbol{0}$. Therefore, thanks to standard results of linear algebra (see [17, App. A, result R.19]), we have $\boldsymbol{B}_3 \odot (\boldsymbol{B}_1^T - \boldsymbol{B}_2^T) \geq \boldsymbol{0}$. This inequality is extended to the associated real symmetric matrices. Then, we have $\Re\{\boldsymbol{B}_3 \odot \boldsymbol{B}_1^T\} - \Re\{\boldsymbol{B}_3 \odot \boldsymbol{B}_2^T\} \geq \boldsymbol{0}$. Therefore, by inversion, we obtain $(\Re\{\boldsymbol{B}_3 \odot \boldsymbol{B}_1^T\})^{-1} - (\Re\{\boldsymbol{B}_3 \odot \boldsymbol{B}_2^T\})^{-1} \leq \boldsymbol{0}$. Consequently, we obtain the following result:

$$\boldsymbol{C}_v^{\text{noncir}} \leq \boldsymbol{C}_v^{\text{cir}}. \tag{51}$$

IV. New CRB for Noncircular Gaussian Distributed and Temporally and Spatially Correlated Signals

In this section, we assume that the transmitted signals $\{\boldsymbol{x}(t)\}_{t=1,2,\ldots,N}$ are zero-mean Gaussian distributed. Then, we introduce the following extended vector $\tilde{\boldsymbol{x}}$:

$$\tilde{\boldsymbol{x}} = \begin{pmatrix}\boldsymbol{x}\\ \boldsymbol{x}^*\end{pmatrix}. \tag{52}$$

Then, we have

$$\tilde{\boldsymbol{x}} \sim \mathcal{N}(\boldsymbol{0}, \tilde{\boldsymbol{\mathcal{P}}}) \tag{53}$$

where

$$\tilde{\boldsymbol{\mathcal{P}}} = \mathrm{E}\left\{\tilde{\boldsymbol{x}}\tilde{\boldsymbol{x}}^H\right\} = \begin{pmatrix}\boldsymbol{\mathcal{P}} & \boldsymbol{\mathcal{P}}'\\ \boldsymbol{\mathcal{P}}'^* & \boldsymbol{\mathcal{P}}^*\end{pmatrix} \tag{54}$$

where $\boldsymbol{\mathcal{P}}$ and $\boldsymbol{\mathcal{P}}'$ are previously defined in (3) and (4), respectively.

To derive the CRB of the considered model, we assume that the noise is circular Gaussian distributed and the noise covariance matrix $\boldsymbol{C}$ is known (possibly up to a multiplicative scalar). Then, we define the parameter vector as follows:

$$\boldsymbol{\alpha} = \left(\boldsymbol{\theta}^T, \boldsymbol{\beta}^T\right)^T$$

where $\boldsymbol{\theta}$, introduced in Section II, represents the directions of the narrowband sources and $\boldsymbol{\beta}$ is defined by

$$\boldsymbol{\beta} = \Bigg(\left(\Re\{\boldsymbol{P}_{ij}\}, \Im\{\boldsymbol{P}_{ij}\}, \Re\{\boldsymbol{P}'_{ij}\}, \Im\{\boldsymbol{P}'_{ij}\}\right)_{1\leq j<i\leq NK},\ \left(\boldsymbol{P}_{ii}, \Re\{\boldsymbol{P}'_{ii}\}, \Im\{\boldsymbol{P}'_{ii}\}\right)_{i=1,\ldots,NK}\Bigg)^T.$$

We also define the vector $\bar{\boldsymbol{y}}_N$ as

$$\bar{\boldsymbol{y}}_N = \left[\boldsymbol{C}^{-\frac{1}{2}}\boldsymbol{y}(1), \ldots, \boldsymbol{C}^{-\frac{1}{2}}\boldsymbol{y}(N)\right]^T.$$

Moreover, we introduce the following extended vector $\tilde{\bar{\boldsymbol{y}}}_N$:

$$\tilde{\bar{\boldsymbol{y}}}_N = \left[\bar{\boldsymbol{y}}_N,\ \bar{\boldsymbol{y}}_N^*\right]^T.$$

Then, we have

$$\tilde{\bar{\boldsymbol{y}}}_N \sim \mathcal{N}(\boldsymbol{0}, \tilde{\boldsymbol{\mathcal{R}}}_N)$$

where

$$\tilde{\boldsymbol{\mathcal{R}}}_N = \mathrm{E}\left\{\tilde{\bar{\boldsymbol{y}}}_N\tilde{\bar{\boldsymbol{y}}}_N^H\right\} = \begin{pmatrix}\boldsymbol{\mathcal{R}}_N & \boldsymbol{\mathcal{R}}'_N\\ \boldsymbol{\mathcal{R}}'^*_N & \boldsymbol{\mathcal{R}}^*_N\end{pmatrix}$$

with

$$\begin{aligned}\boldsymbol{\mathcal{R}}_N &= \mathrm{E}\left\{\bar{\boldsymbol{y}}_N\bar{\boldsymbol{y}}_N^H\right\}\\ \boldsymbol{\mathcal{R}}'_N &= \mathrm{E}\left\{\bar{\boldsymbol{y}}_N\bar{\boldsymbol{y}}_N^T\right\}.\end{aligned}$$

$\boldsymbol{\mathcal{R}}_N$ and $\boldsymbol{\mathcal{R}}'_N$ can be written as

$$\begin{aligned}\boldsymbol{\mathcal{R}}_N &= \bar{\boldsymbol{G}}\boldsymbol{\mathcal{P}}\bar{\boldsymbol{G}}^H + \boldsymbol{I}_{NL}\\ \boldsymbol{\mathcal{R}}'_N &= \bar{\boldsymbol{G}}\boldsymbol{\mathcal{P}}'\bar{\boldsymbol{G}}^H\end{aligned}$$

where $\bar{\boldsymbol{G}}$ is defined as follows:

$$\bar{\boldsymbol{G}} = \boldsymbol{I}_N \otimes \left(\boldsymbol{C}^{-\frac{1}{2}}\boldsymbol{A}\right).$$

Therefore, $\tilde{\boldsymbol{\mathcal{R}}}_N$ is rewritten as

$$\tilde{\boldsymbol{\mathcal{R}}}_N = \tilde{\bar{\boldsymbol{G}}}\tilde{\boldsymbol{\mathcal{P}}}\tilde{\bar{\boldsymbol{G}}}^H + \boldsymbol{I}_{2NL}$$

where

$$\tilde{\bar{\boldsymbol{G}}} = \begin{pmatrix}\bar{\boldsymbol{G}} & \boldsymbol{0}_{NL\times NK}\\ \boldsymbol{0}_{NL\times NK} & \bar{\boldsymbol{G}}^*\end{pmatrix}.$$

Similarly to [18], the ikth entry of the Fisher information matrix (FIM) corresponding to $\tilde{\bar{\boldsymbol{y}}}_N$ is given by

$$[\boldsymbol{I}_{\mathrm{F}}]_{ik} = [\mathrm{CRB}]_{ik}^{-1} = \frac{1}{2}\mathrm{tr}\left(\frac{\partial\tilde{\boldsymbol{\mathcal{R}}}_N}{\partial\alpha_i}\tilde{\boldsymbol{\mathcal{R}}}_N^{-1}\frac{\partial\tilde{\boldsymbol{\mathcal{R}}}_N}{\partial\alpha_k}\tilde{\boldsymbol{\mathcal{R}}}_N^{-1}\right).$$

Following the same steps of [19], we obtain the following expression of $[\mathrm{CRB}]_{ik}^{-1}$:

$$[\mathrm{CRB}]_{ik}^{-1} = \Re\left\{\mathrm{tr}\left(\tilde{\bar{\boldsymbol{G}}}_i^H\boldsymbol{\Pi}_{\tilde{\bar{\boldsymbol{G}}}}^{\perp}\tilde{\bar{\boldsymbol{G}}}_k\tilde{\boldsymbol{\mathcal{P}}}\tilde{\bar{\boldsymbol{G}}}^H\tilde{\boldsymbol{\mathcal{R}}}_N^{-1}\tilde{\bar{\boldsymbol{G}}}\tilde{\boldsymbol{\mathcal{P}}}\right)\right\}$$

where

$$\begin{aligned}\tilde{\bar{\boldsymbol{G}}}_i &= \frac{\partial\tilde{\bar{\boldsymbol{G}}}(\boldsymbol{\theta})}{\partial\theta_i}\\ \boldsymbol{\Pi}_{\tilde{\bar{\boldsymbol{G}}}}^{\perp} &= \boldsymbol{I}_{2NL} - \tilde{\bar{\boldsymbol{G}}}\left(\tilde{\bar{\boldsymbol{G}}}^H\tilde{\bar{\boldsymbol{G}}}\right)^{-1}\tilde{\bar{\boldsymbol{G}}}^H.\end{aligned}$$

Some algebraic manipulations (see Appendix C) yield the following expression of $\mathrm{CRB}(\boldsymbol{\theta})$ for temporally correlated signals generated from noncircular sources

$$\mathrm{CRB}^{\frac{\text{noncir}}{\text{cor}}}(\boldsymbol{\theta}) = \frac{1}{2}\left[\Re\left\{\left(\boldsymbol{D}^H\boldsymbol{C}^{-\frac{1}{2}}\boldsymbol{\Pi}_{\bar{\boldsymbol{G}}}^{\perp}\boldsymbol{C}^{-\frac{1}{2}}\boldsymbol{D}\right)\odot \mathrm{Btr}_K\left(\begin{pmatrix}\boldsymbol{\mathcal{P}}\boldsymbol{\mathcal{A}}^H & \boldsymbol{\mathcal{P}}'\boldsymbol{\mathcal{A}}^T\end{pmatrix}\tilde{\boldsymbol{\mathcal{R}}}^{-1}\begin{pmatrix}\boldsymbol{\mathcal{A}}\boldsymbol{\mathcal{P}}\\ \boldsymbol{\mathcal{A}}^*\boldsymbol{\mathcal{P}}'^*\end{pmatrix}\right)^T\right\}\right]^{-1} \tag{55}$$

where $\boldsymbol{\mathcal{A}}$ is defined in (11). We note here that in the case of circular sources, we have $\boldsymbol{\mathcal{P}}' = \mathbf{0}_{KN\times KN}$ and $\boldsymbol{\mathcal{R}}' = \mathbf{0}_{LN\times LN}$. Therefore, $\tilde{\boldsymbol{\mathcal{R}}}$ becomes

$$\tilde{\boldsymbol{\mathcal{R}}} = \begin{pmatrix} \boldsymbol{\mathcal{R}} & \mathbf{0}_{LN\times LN} \\ \mathbf{0}_{LN\times LN} & \boldsymbol{\mathcal{R}}^* \end{pmatrix}.$$

Consequently, (55) reduces to

$$\mathrm{CRB}^{\frac{\mathrm{cir}}{\mathrm{cor}}}(\boldsymbol{\theta}) = \frac{1}{2}\left[\Re\left\{\left(\boldsymbol{D}^H\boldsymbol{C}^{-\frac{1}{2}}\boldsymbol{\Pi}^{\perp}_{\boldsymbol{G}}\boldsymbol{C}^{-\frac{1}{2}}\boldsymbol{D}\right)\odot \mathrm{Btr}_K\left(\boldsymbol{\mathcal{P}}\boldsymbol{\mathcal{A}}^H\boldsymbol{\mathcal{R}}^{-1}\boldsymbol{\mathcal{A}}\boldsymbol{\mathcal{P}}\right)^T\right\}\right]^{-1} \quad (56)$$

derived in [13].

Now, we denote

$$\boldsymbol{B}_1 = \begin{pmatrix}\boldsymbol{\mathcal{P}}\boldsymbol{\mathcal{A}}^H & \boldsymbol{\mathcal{P}}'\boldsymbol{\mathcal{A}}^T\end{pmatrix}\tilde{\boldsymbol{\mathcal{R}}}^{-1}\begin{pmatrix}\boldsymbol{\mathcal{A}}\boldsymbol{\mathcal{P}} \\ \boldsymbol{\mathcal{A}}^*\boldsymbol{\mathcal{P}}'^*\end{pmatrix}$$
$$\boldsymbol{B}_2 = \boldsymbol{\mathcal{P}}\boldsymbol{\mathcal{A}}^H\boldsymbol{\mathcal{R}}^{-1}\boldsymbol{\mathcal{A}}\boldsymbol{\mathcal{P}}$$
$$\boldsymbol{B}_3 = \boldsymbol{D}^H\boldsymbol{C}^{-\frac{1}{2}}\boldsymbol{\Pi}^{\perp}_{\boldsymbol{G}}\boldsymbol{C}^{-\frac{1}{2}}\boldsymbol{D}.$$

Applying [1, Lemma A.4] to $\boldsymbol{B}_1$ and $\boldsymbol{B}_2$, we obtain $\boldsymbol{B}_1 \geq \boldsymbol{B}_2$. This inequality applies to the transpose of these matrices. Then, we have $\boldsymbol{B}_1^T - \boldsymbol{B}_2^T \geq \mathbf{0}$. Moreover, we have $\boldsymbol{B}_3 \geq \mathbf{0}$. Therefore, thanks to standard results of linear algebra (see [17, App. A, result R.19]), we have $\boldsymbol{B}_3 \odot (\boldsymbol{B}_1^T - \boldsymbol{B}_2^T) \geq \mathbf{0}$. This inequality is extended to the associated real symmetric matrices. Then, we have $\Re\{\boldsymbol{B}_3 \odot \boldsymbol{B}_1^T\} - \Re\{\boldsymbol{B}_3 \odot \boldsymbol{B}_2^T\} \geq \mathbf{0}$. Therefore, by inversion, we obtain $(\Re\{\boldsymbol{B}_3 \odot \boldsymbol{B}_1^T\})^{-1} - (\Re\{\boldsymbol{B}_3 \odot \boldsymbol{B}_2^T\})^{-1} \leq \mathbf{0}$. Consequently, we obtain the following result:

$$\mathrm{CRB}^{\frac{\mathrm{noncir}}{\mathrm{cor}}}(\boldsymbol{\theta}) \leq \mathrm{CRB}^{\frac{\mathrm{cir}}{\mathrm{cor}}}(\boldsymbol{\theta}). \quad (57)$$

V. Graphical Representations

In this section, we will present some figures to illustrate the application of the new extended version of the two-sided IV-SSF method and compare it to the two-sided IV-SSF method derived in [16] for circular sources (referred to as circular method) and to the MODE method derived in [1]. Throughout this section, we consider a zero-mean, Gaussian distributed and temporally white noise. We also consider a uniform linear array of four sensors separated by a half-wavelength. The number of instrumental variables is $M = 2$. Moreover, 10 000 independent simulation runs have been performed to obtain the estimated DOAs. The signal temporal correlation is simulated via filtering the complex noncircular Gaussian signals with an FIR filter with relative tap weights

$$f(z) = 1 + 0.5z^{-1} + 0.3z^{-2} + 0.2z^{-3} + 0.1z^{-4} \quad (58)$$

which is then normalized to give a unit-energy filter. The DOAs estimate are calculated using a coarse search with finely grid size 0.001.

A. Case of Spatially Correlated Noise

In the first subsection, we consider the case of spatially correlated noise to compare our new extended two-sided IV-SSF method to the classical two-sided IV-SSF one. The noise is then assumed to have klth element as follows:

$$\boldsymbol{C}_{kl} = \sigma^2 0.9^{|k-l|}e^{j\frac{\pi}{2}(k-l)}.$$

Note here that the MODE method is not included in this subsection because it is applicable only for both temporally and spatially uncorrelated noise. Therefore, the MODE algorithm will be included in the next subsection where we will consider the case of spatially uncorrelated noise.

We first consider two spatially uncorrelated equipowered complex noncircular Gaussian signals with identical noncircularity rate ρ and noncircularity phase $\phi = \frac{\pi}{2}$. The two uncorrelated sources are located at $\theta_1 = 0.2$ and $\theta_2 = 0.4$ radians with respect to the normal of the array broadside.

To compare the performance of our extended two-sided IV-SSF method to the corresponding CRB, we should first evaluate the bias of the estimates of θ_1 of our new method. In Fig. 1, the bias of the estimates of θ_1 of our extended two-sided IV-SSF method is presented versus the SNR for $N = 100$ snapshots at $\rho = 1$ and compared to that of the circular version. We see from Fig. 1 that the bias becomes negligible, especially at high SNR values for both versions. Therefore, it is still meaningful to compare the performance of the extended and the circular methods to the square root of the $\mathrm{CRB}^{\frac{\mathrm{noncir}}{\mathrm{cor}}}$ and $\mathrm{CRB}^{\frac{\mathrm{cir}}{\mathrm{cor}}}$, respectively. To represent these CRBs, we define the first and the second (unconjugated) signal space-time covariance matrices as follows:

$$\boldsymbol{\mathcal{P}} = \boldsymbol{P}_t \otimes \boldsymbol{P}$$
$$\boldsymbol{\mathcal{P}}' = \boldsymbol{P}_t \otimes \boldsymbol{P}'$$

where $\boldsymbol{P}$ and $\boldsymbol{P}'$ are the covariance matrices of the two noncircular complex Gaussian signals. Moreover, $\boldsymbol{P}_t$ represents the temporal correlation matrix computed using (58). In Fig. 2, the standard deviation of the estimates of θ_1 of our extended two-sided IV-SSF method is presented versus the SNR for $N = 100$ snapshots at $\rho = 1$ and compared to that of the circular version and to the corresponding CRB. We see from this figure that the extended two-sided IV-SSF outperforms the circular version in terms of lower standard deviation. This confirms the inequality given in (51). Moreover, the improvement made by our extended two-sided IV-SSF is more pronounced at low SNR values. We also verify that

$$\mathrm{CRB}^{\frac{\mathrm{noncir}}{\mathrm{cor}}} < \mathrm{STD}^{\text{extended method}}$$
$$\mathrm{CRB}^{\frac{\mathrm{cir}}{\mathrm{cor}}} < \mathrm{STD}^{\text{circular method}}.$$

Otherwise, we confirm the inequality given in (57). Finally, we see that

$$\lim_{\mathrm{SNR}\longrightarrow+\infty}\mathrm{CRB}^{\frac{\mathrm{noncir}}{\mathrm{cor}}} = \lim_{\mathrm{SNR}\longrightarrow+\infty}\mathrm{CRB}^{\frac{\mathrm{cir}}{\mathrm{cor}}}.$$

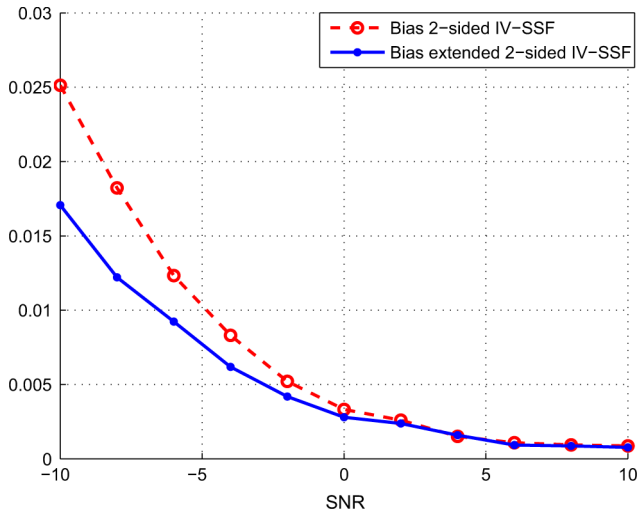

Fig. 1. Bias of the extended and circular two-sided IV-SSF methods versus SNR for $N = 100$ and $\rho = 1$.

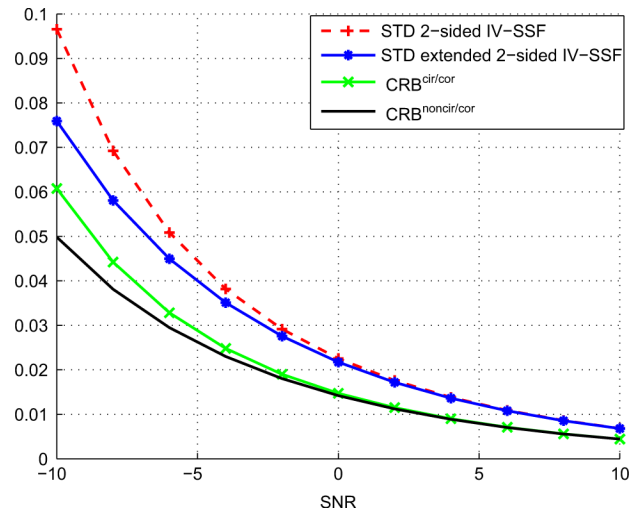

Fig. 2. Comparison of the standard deviation of the extended and circular two-sided IV-SSF methods to the corresponding CRBs versus SNR for $N = 100$ and $\rho = 1$.

Now, Fig. 3 represents the ratio $r_1 = \frac{\text{STD}^{\text{extended method}}}{\text{STD}^{\text{circular method}}}$ as a function of the noncircularity rate ρ. We notice from Fig. 3 that the improvement made by the extended two-sided IV-SSF method increases as the noncircularity rate increases. Moreover, this improvement is more prominent at low SNR values. Next, we assume that the two sources are strongly spatially correlated with correlation coefficient $\rho_{\text{co}} = 0.98$. In Fig. 4, the standard deviation and the CRB of the estimates of θ_1 of our extended two-sided IV-SSF method is presented versus the SNR for $N = 100$ snapshots at $\rho = 1$ and compared to that of the circular version. We see from this figure that the extended two-sided IV-SSF outperforms slightly the circular version in terms of standard deviation for spatially correlated sources. Then, we conclude that the improvement made by the extended two-sided IV-SSF method with regard to the circular method is more prominent for the spatially uncorrelated sources case.

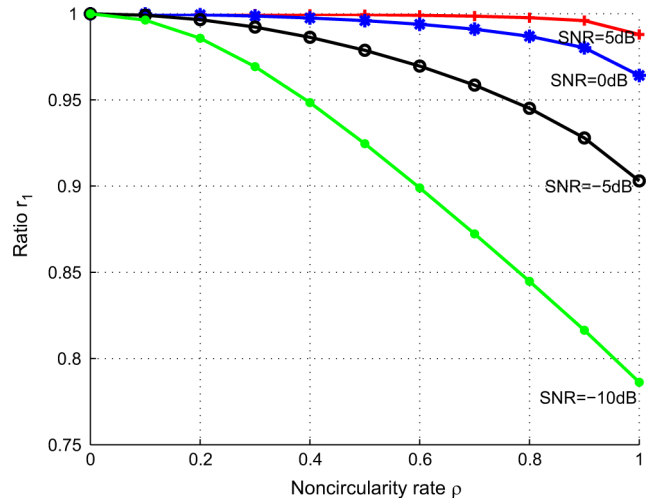

Fig. 3. $r_1 = \frac{\text{STD}^{\text{extended method}}}{\text{STD}^{\text{circular method}}}$ as a function of the noncircularity rate ρ, for $SNR = 0$ dB and $N = 100$.

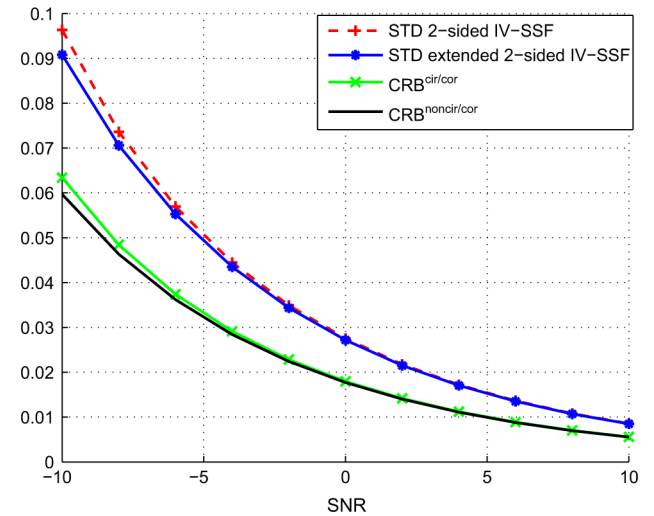

Fig. 4. Standard deviation of the extended and circular two-sided IV-SSF methods and the corresponding CRBs versus SNR for strongly spatially correlated signals, $N = 100$ and $\rho = 1$.

B. Case of Spatially Uncorrelated Noise

To compare the extended and the circular two-sided IV-SSF methods to the MODE method, we suppose that the noise is spatially uncorrelated. As done in the first subsection, we first consider the scenario of two uncorrelated sources located at $\theta_1 = 0.2$ and $\theta_2 = 0.4$ radians with respect to the normal of the array broadside. In Fig. 5, the standard deviation of the estimates of θ_1 of our extended two-sided IV-SSF method is presented versus the SNR for $N = 100$ snapshots at $\rho = 1$ and compared to that of the circular version and the MODE method. We see from Fig. 5 that the MODE method outperforms the classical two-sided IV-SSF method. However, the extended two-sided IV-SSF method is statistically more efficient than the MODE estimator for low SNR values. Next, in Fig. 6, we assume that the signals are spatially correlated with correlation coefficients 0.5. It can be seen from Fig. 6 that our extended method also outperforms the MODE estimator for partly correlated sources. Now, in Fig. 7, we assume that the two sources

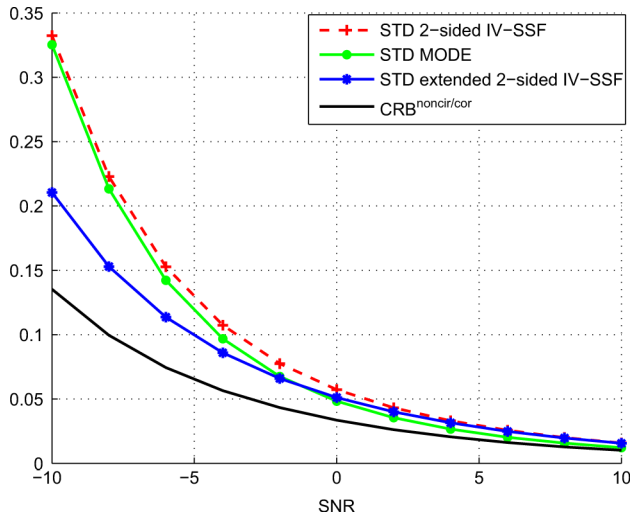

Fig. 5. Comparison of the standard deviation of the extended and circular two-sided IV-SSF methods to that of the MODE method versus SNR for spatially uncorrelated signals, $N = 100$ and $\rho = 1$.

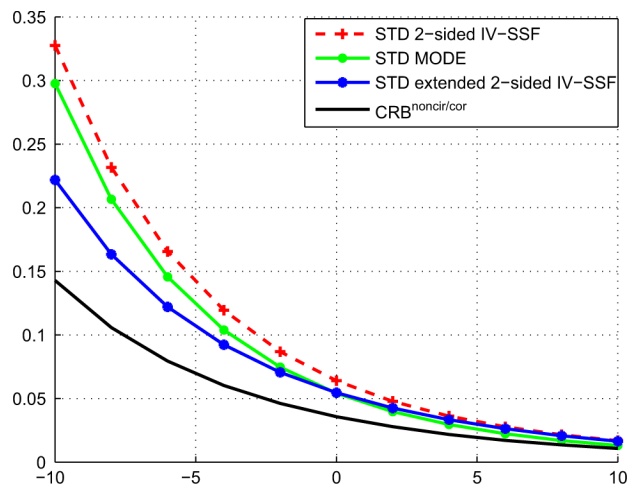

Fig. 6. Standard deviation of the extended and circular two-sided IV-SSF methods versus SNR for partly correlated signals, $N = 100$ and $\rho = 1$.

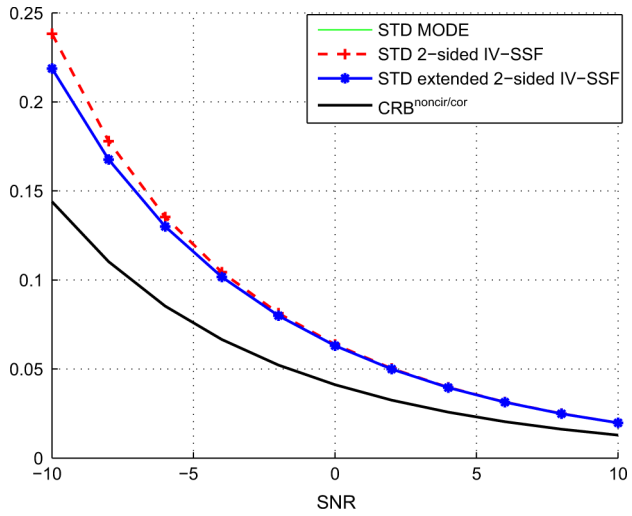

Fig. 7. Standard deviation of the extended and circular two-sided IV-SSF methods versus SNR for fully coherent signals, $N = 100$ and $\rho = 1$.

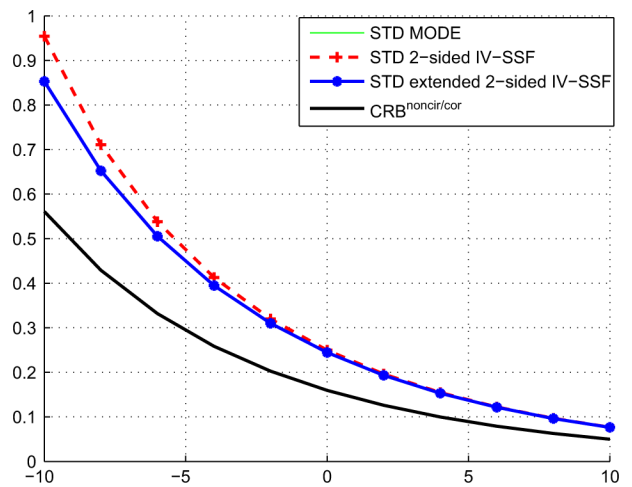

Fig. 8. Standard deviation of the extended and circular two-sided IV-SSF methods versus SNR for partly coherent signals, $N = 100$ and $\rho = 1$.

are fully correlated (fully coherent). It can be clearly seen from Fig. 7 that for fully coherent sources the MODE method fails completely to estimate the DOA while the extended and the circular two-sided IV-SSF methods are able to estimate the DOA with almost equivalent performance. Finally, we consider in Fig. 8 three partly coherent equipowered complex noncircular Gaussian sources (the two first sources are spatially fully correlated but spatially uncorrelated with the last source) with identical noncircularity rate ρ and noncircularity phase $\phi = \frac{\pi}{2}$. The three sources are located at $\theta_1 = 0.2$, $\theta_2 = 0.4$, and $\theta_3 = 0.6$ radians with respect to the normal of the array broadside. It can be also seen from Fig. 8 that only the extended and the circular two-sided IV-SSF methods accommodate the case of partly coherent signals. We note here that although the extended two-sided IV-SSF method is computationally more demanding than the classical two-sided IV-SSF and the MODE methods, it is statistically more efficient especially in the case of partly and fully coherent signals.

Now, we will see that the CRB obtained assuming both noncircular sources and temporally correlated signals is lower than the CRBs derived considering only one of these two assumptions. We first consider two equipowered sources with identical noncircularity rate $\rho = 1$ and noncircularity phases $\phi_1 = \frac{\pi}{2}$ and $\phi_2 = \frac{\pi}{3}$. These sources, located at angles $\theta_1 = 0$ and $\theta_2 = 0.2$ radians with respect to the normal of array broadside, impinge on a uniform linear array of sensors separated by a half-wavelength for which

$$\boldsymbol{a}(\theta_k) = \left[1, e^{j\pi \sin(\theta_k)}, e^{2j\pi \sin(\theta_k)}, \ldots, e^{j(M-1)\pi \sin(\theta_k)}\right]^T$$

where $\{\theta_k\}_{k=1,2}$ are the DOAs relative to the normal of the array broadside. The number of the array sensors is 4 and the SNR $= 0$ dB. We suppose that the signals are spatially uncorrelated and we consider the first and the second covariance matrices and the temporal correlation matrices as follows:

$$[\boldsymbol{P}]_{ij} = \delta_{ij}$$
$$[\boldsymbol{P}']_{ij} = \rho e^{j\phi_i}\delta_{ij}$$
$$[\boldsymbol{P}_t]_{ij} = e^{-0.2|i-j|}.$$

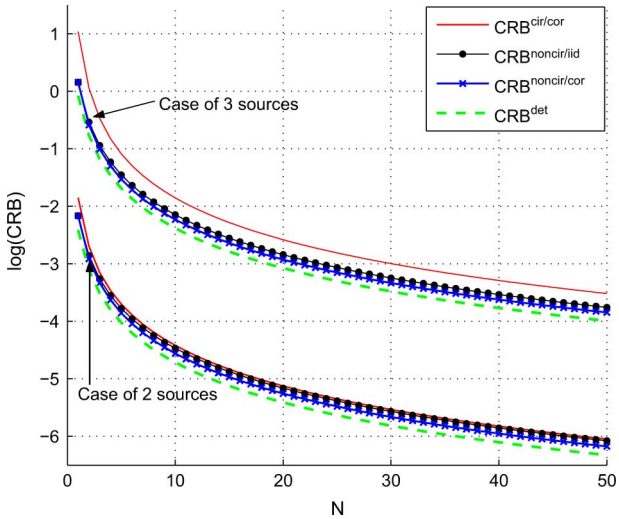

Fig. 9. An example of the CRBs versus the number of snapshots N in logarithmic scale at $SNR = 0$ dB and $\rho = 1$.

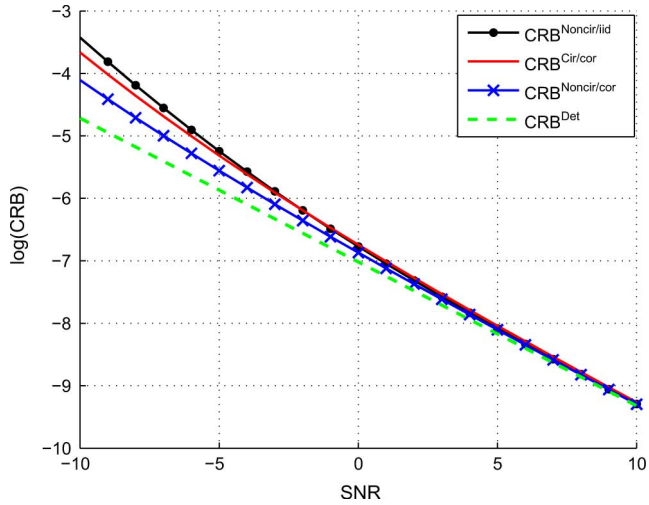

Fig. 10. An example of the CRBs versus the SNR in logarithmic scale for two equipowered sources and number of snapshots $N = 100$.

We also consider the noise covariance matrix as follows:

$$[\boldsymbol{C}]_{ij} = \sigma^2 e^{|i-j|}.$$

Fig. 9 shows $\log(\mathrm{CRB}^{\frac{\mathrm{noncir}}{\mathrm{cor}}})$, $\log(\mathrm{CRB}^{\frac{\mathrm{cir}}{\mathrm{cor}}})$, $\log(\mathrm{CRB}^{\frac{\mathrm{noncir}}{\mathrm{uncor}}})$ and the deterministic CRB $\log(\mathrm{CRB}^{\mathrm{det}})$ as a function of the number of snapshots N. From Fig. 9 we verify that

$$\mathrm{CRB}^{\mathrm{det}} \leq \mathrm{CRB}^{\frac{\mathrm{noncir}}{\mathrm{cor}}} \leq \mathrm{CRB}^{\frac{\mathrm{cir}}{\mathrm{cor}}} \quad (59)$$

$$\mathrm{CRB}^{\frac{\mathrm{noncir}}{\mathrm{cor}}} \leq \mathrm{CRB}^{\frac{\mathrm{noncir}}{\mathrm{noncor}}}. \quad (60)$$

We also verify that the CRB obtained assuming both noncircular sources and temporally correlated signals is lower than the CRBs derived considering only one of these two assumptions. This illustrates the potential gain that both the noncircularity and the temporal correlation offer when considered together. Moreover, we see from Fig. 9 that the difference between these CRBs increases with the number of snapshots N. This is hardly surprising since the more samples we receive, the more information we can retrieve about the temporal correlation and the noncircularity of the signals. In fact, by increasing the number of snapshots N, there is more room for both the noncircularity of the signals and the temporal correlation to improve the DOA estimation performance. Now, we consider in the same figure three equipowered sources with identical noncircularity rate $\rho = 1$ and noncircularity phases $\phi_1 = \frac{\pi}{2}$, $\phi_2 = \frac{\pi}{2}$, and $\phi_3 = \frac{\pi}{3}$. These sources are located at angles $\theta_1 = 0$, $\theta_2 = 0.2$ and $\theta_3 = 0.4$ radians. We confirm the inequalities (59) and (60). Moreover, we prove that the difference between $\mathrm{CRB}^{\frac{\mathrm{noncir}}{\mathrm{cor}}}$ and $\mathrm{CRB}^{\frac{\mathrm{cir}}{\mathrm{cor}}}$ increases with the number of sources K while the difference between $\mathrm{CRB}^{\frac{\mathrm{noncir}}{\mathrm{cor}}}$ and $\mathrm{CRB}^{\frac{\mathrm{noncir}}{\mathrm{noncor}}}$ decreases as K increases. This can be explained by the fact that when K increases, there is more room for the noncircularity of the signals to improve the DOA estimation performance than the temporal correlation.

In the following graphical representations, we reconsider the case of two equipowered sources. In Fig. 10, the CRBs are depicted versus the SNR. It can be seen from Fig. 10 that as the SNR increases, the CRBs merge together and decrease linearly. In fact, at high SNR values, the useful signals are not too much corrupted by noise. Then, in this SNR region, the signals are very informative about the DOA estimates. This scenario is therefore equivalent to the deterministic case. This illustrates the fact that at high SNR values, all the CRBs coincide. Moreover, at low SNR values, we notice that the temporal correlation is more informative about the unknown DOA parameters than the noncircularity. In fact, at low SNR values, the useful signals are too much corrupted by noise. Therefore, they are not very informative about the unknown DOA and more particularly, the noncircularity rate does not bring much more information about the DOA estimates.

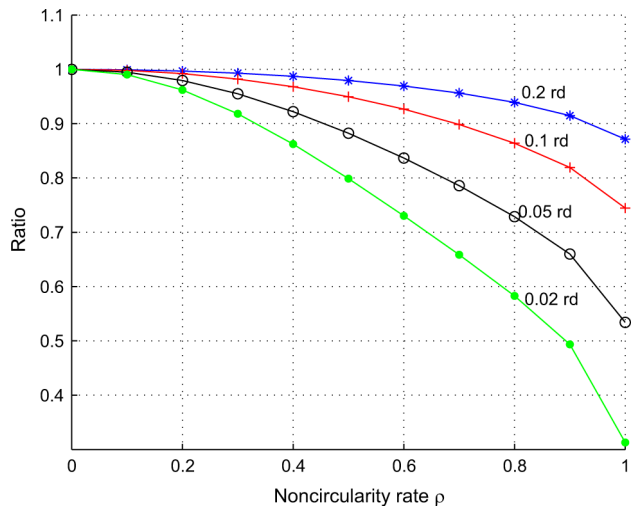

Fig. 11. $\mathrm{Ratio} = \left(\mathrm{CRB}^{\frac{\mathrm{noncir}}{\mathrm{cor}}}\right) / \left(\mathrm{CRB}^{\frac{\mathrm{cir}}{\mathrm{cor}}}\right)$ as a function of the noncircularity rate ρ for different values of DOA separation $(\Delta\theta)$, for $\phi_1 = \frac{\pi}{2}, \phi_2 = \frac{\pi}{3}$, $N = 100$ and $SNR = 0$ dB.

In Figs. 11 and 12, we show the dependence of the $\mathrm{CRB}^{\frac{\mathrm{noncir}}{\mathrm{cor}}}$ on the noncircularity rate ρ , the circularity phase separation $\Delta\phi = \phi_2 - \phi_1$ and the DOA separation $\Delta\theta = \theta_2 - \theta_1$.

In fact, Fig. 11 represents the ratio

$$\frac{\left(\mathrm{CRB}^{\frac{\mathrm{noncir}}{\mathrm{cor}}}\right)}{\left(\mathrm{CRB}^{\frac{\mathrm{cir}}{\mathrm{cor}}}\right)}$$

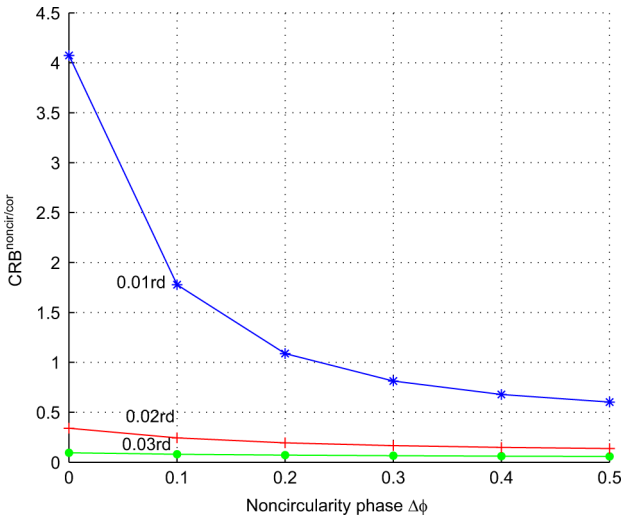

Fig. 12. $\mathrm{CRB}^{\frac{\mathrm{noncir}}{\mathrm{cor}}}$ as a function of the noncircularity phase $\Delta\phi$ for different values of DOA separation ($\Delta\theta$) for $\rho = 1$, $N = 100$ and $SNR = 0$ dB.

as a function of the noncircularity rate for different values of $\Delta\theta$. It can be seen from this figure that $\mathrm{CRB}^{\frac{\mathrm{noncir}}{\mathrm{cor}}}$ decreases as the noncircularity rate increases and this decrease is more prominent at low DOA separations. Moreover, from Fig. 12, we see that the $\mathrm{CRB}^{\frac{\mathrm{noncir}}{\mathrm{cor}}}$ is sensitive to the circularity phase separation at low DOA separations.

VI. Conclusion

In this paper, we developed for the first time a method for estimating the DOA parameters assuming noncircular and temporally and spatially correlated signals. The new proposed method extends the well-known two-sided IV-SSF approach to noncircular and time-correlated signals. We proved that this new method outperforms the classical two-sided IV-SSF technique in terms of lower bias and error variance. Moreover, the new method is statistically more efficient than the MODE method especially in the case of partly and fully correlated signals where only the extended and the classical two-sided IV-SSF methods are applicable. We also derived an explicit expression for the stochastic Cramér–Rao bound (CRB) of the DOA estimates for temporally and spatially correlated signals generated from noncircular sources. This CRB was compared to those of circular temporally correlated and noncircular independent and identically distributed signals. We showed the potential gain that both noncircularity and temporal correlation provide when considered together. We also proved that the difference between the three CRBs increases with the number of snapshots. On the other hand, as the SNR increases, the CRBs merge together and decrease linearly. Furthermore, at low SNR values we showed that the temporal correlation is more informative about the unknown DOA parameters than the noncircularity. Finally, we proved that the CRB derived assuming noncircular and temporally-correlated signals decreases as the noncircularity rate increases. Furthermore, this decrease is more prominent at low DOA separations where the CRB is sensitive to the noncircularity phase separation.

Appendix A
Derivation of $\boldsymbol{H}$

We denote $\tilde{\boldsymbol{G}} = \tilde{\boldsymbol{C}}^{-\frac{1}{2}}\tilde{\boldsymbol{A}}$. Then, we have

$$\tilde{\boldsymbol{\Pi}}_0^{\perp} = \boldsymbol{\Pi}_{\tilde{\boldsymbol{G}}}^{\perp}.$$

We also introduce the following notations:

$$\tilde{\boldsymbol{G}}^{\dagger} = \left(\tilde{\boldsymbol{G}}^H\tilde{\boldsymbol{G}}\right)^{-1}\tilde{\boldsymbol{G}}^H$$
$$\tilde{\boldsymbol{A}}^{\dagger} = \left(\tilde{\boldsymbol{A}}^H\tilde{\boldsymbol{A}}\right)^{-1}\tilde{\boldsymbol{A}}^H.$$

Starting from (47) and after tedious algebraic manipulations, we obtain the following expression for the ikth entry of the limiting Hessian matrix:

$$[\boldsymbol{H}]_{ik} = 2\Re\left\{\mathrm{tr}\left(\tilde{\boldsymbol{G}}_i^H\tilde{\boldsymbol{\Pi}}_0^{\perp}\tilde{\boldsymbol{G}}_k\tilde{\boldsymbol{G}}^{\dagger}\tilde{\boldsymbol{C}}^{-\frac{1}{2}}\tilde{\boldsymbol{V}}_s\tilde{\boldsymbol{\Delta}}_s^2\tilde{\boldsymbol{V}}_s^H\tilde{\boldsymbol{C}}^{-\frac{1}{2}}\tilde{\boldsymbol{G}}^{\dagger H}\right)\right\} \tag{61}$$

where

$$\boldsymbol{G}_i = \frac{\partial \boldsymbol{G}(\boldsymbol{\theta})}{\partial\theta_i}.$$

Otherwise, we have $\tilde{\boldsymbol{V}}_s = \tilde{\boldsymbol{A}}(\boldsymbol{\theta})\boldsymbol{T}$. Then, we obtain $\tilde{\boldsymbol{G}}^{\dagger}\tilde{\boldsymbol{C}}^{-\frac{1}{2}}\tilde{\boldsymbol{V}}_s = \tilde{\boldsymbol{G}}^{\dagger}\tilde{\boldsymbol{G}}\boldsymbol{T} = \boldsymbol{T} = \tilde{\boldsymbol{A}}^{\dagger}\tilde{\boldsymbol{V}}_s$. Consequently, (61) can be written as

$$\boldsymbol{H}_{ik} = 2\Re\left\{\mathrm{tr}\left(\tilde{\boldsymbol{D}}_i^H\tilde{\boldsymbol{C}}^{-\frac{1}{2}}\tilde{\boldsymbol{\Pi}}_0^{\perp}\tilde{\boldsymbol{C}}^{-\frac{1}{2}}\tilde{\boldsymbol{D}}_k\tilde{\boldsymbol{A}}^{\dagger}\tilde{\boldsymbol{V}}_s\tilde{\boldsymbol{\Delta}}_s^2\tilde{\boldsymbol{V}}_s^H\tilde{\boldsymbol{A}}^{\dagger H}\right)\right\}$$

where

$$\tilde{\boldsymbol{D}}_i = \begin{pmatrix}\boldsymbol{D}_i & \boldsymbol{0}_{L\times K}\\ \boldsymbol{0}_{L\times K} & \boldsymbol{D}_i^*\end{pmatrix}.$$

Moreover, we have

$$\tilde{\boldsymbol{G}} = \tilde{\boldsymbol{C}}^{-\frac{1}{2}}\tilde{\boldsymbol{A}},$$
$$= \begin{pmatrix}\boldsymbol{C}^{-\frac{1}{2}}\boldsymbol{A} & \boldsymbol{0}_{L\times K}\\ \boldsymbol{0}_{L\times K} & \left(\boldsymbol{C}^{-\frac{1}{2}}\boldsymbol{A}\right)^*\end{pmatrix} = \begin{pmatrix}\boldsymbol{G} & \boldsymbol{0}_{L\times K}\\ \boldsymbol{0}_{L\times K} & \boldsymbol{G}^*\end{pmatrix}.$$

Therefore, $\tilde{\boldsymbol{\Pi}}_0^{\perp}$ can be written as

$$\tilde{\boldsymbol{\Pi}}_0^{\perp} = \begin{pmatrix}\boldsymbol{\Pi}_0^{\perp} & \boldsymbol{0}_{L\times L}\\ \boldsymbol{0}_{L\times L} & \boldsymbol{\Pi}_0^{\perp *}\end{pmatrix}.$$

Consequently, we obtain the following expression of $[\boldsymbol{H}]_{ik}$:

$$[\boldsymbol{H}]_{ik} =$$
$$2\Re\left\{\mathrm{tr}\left(\begin{pmatrix}\boldsymbol{D}_i^H\boldsymbol{C}^{-\frac{1}{2}}\boldsymbol{\Pi}_0^{\perp}\boldsymbol{C}^{-\frac{1}{2}}\boldsymbol{D}_k & \boldsymbol{0}_{K\times K}\\ \boldsymbol{0}_{K\times K} & \left(\boldsymbol{D}_i^H\boldsymbol{C}^{-\frac{1}{2}}\boldsymbol{\Pi}_0^{\perp}\boldsymbol{C}^{-\frac{1}{2}}\boldsymbol{D}_k\right)^*\end{pmatrix},\right.\right.$$
$$\left.\left.\times\,\tilde{\boldsymbol{A}}^{\dagger}\tilde{\boldsymbol{V}}_s\tilde{\boldsymbol{\Delta}}_s^2\tilde{\boldsymbol{V}}_s^H\tilde{\boldsymbol{A}}^{\dagger H}\right)\right\}.$$

We also have $\tilde{\boldsymbol{V}}_s\tilde{\boldsymbol{\Delta}}_s^2\tilde{\boldsymbol{V}}_s^H = \tilde{\boldsymbol{\Sigma}}^H\tilde{\boldsymbol{\Phi}}^{-1}\tilde{\boldsymbol{\Sigma}}$. Then, from (26) and using the fact that $\tilde{\boldsymbol{A}}^\dagger\tilde{\boldsymbol{A}} = \boldsymbol{I}_{2K}$, we obtain

$$\tilde{\boldsymbol{A}}^\dagger\tilde{\boldsymbol{V}}_s\tilde{\boldsymbol{\Delta}}_s^2\tilde{\boldsymbol{V}}_s^H\tilde{\boldsymbol{A}}^{\dagger H} = \tilde{\boldsymbol{\mathcal{J}}}^H\tilde{\boldsymbol{\mathcal{A}}}_M^H\tilde{\boldsymbol{\Phi}}^{-1}\tilde{\boldsymbol{\mathcal{A}}}_M\tilde{\boldsymbol{\mathcal{J}}}.$$

Now, we consider that

$$\boldsymbol{\mathcal{J}} = [\boldsymbol{C}_{l1},\ldots,\boldsymbol{C}_{li},\ldots,\boldsymbol{C}_{lK}]$$
$$\boldsymbol{\mathcal{J}}' = [\boldsymbol{C}'_{l1},\ldots,\boldsymbol{C}'_{li},\ldots,\boldsymbol{C}'_{lK}]$$

where $\{\boldsymbol{C}_{li}\}_{KM\times 1}$ and $\{\boldsymbol{C}'_{li}\}_{KM\times 1}$ are the i^{th} columns of $\boldsymbol{\mathcal{J}}$ and $\boldsymbol{\mathcal{J}}'$, respectively. Otherwise, we have

$$\boldsymbol{D}_i = (\boldsymbol{0}_{L\times 1},\ldots,\boldsymbol{d}_i,\ldots,\boldsymbol{0}_{L\times 1}).$$

Therefore, we obtain the following expression of $[\boldsymbol{H}]_{ik}$:

$$\begin{aligned}[\boldsymbol{H}]_{ik} &= 2\Re\Bigg\{\mathrm{tr}\Bigg(\begin{pmatrix}\boldsymbol{d}_i^H\boldsymbol{C}^{-\frac{1}{2}}\boldsymbol{\Pi}_0^\perp\boldsymbol{C}^{-\frac{1}{2}}\boldsymbol{d}_k & 0\\ 0 & \left(\boldsymbol{d}_i^H\boldsymbol{C}^{-\frac{1}{2}}\boldsymbol{\Pi}_0^\perp\boldsymbol{C}^{-\frac{1}{2}}\boldsymbol{d}_k\right)^*\end{pmatrix}\\ &\quad\times\begin{pmatrix}\boldsymbol{C}_{lk}^H & \boldsymbol{C}'_{lk}{}^T\\ \boldsymbol{C}'_{lk}{}^H & \boldsymbol{C}_{lk}^T\end{pmatrix}\begin{pmatrix}\boldsymbol{\mathcal{A}}_M^H & \boldsymbol{0}_{KM\times LM}\\ \boldsymbol{0}_{KM\times LM} & \boldsymbol{\mathcal{A}}_M^T\end{pmatrix}\tilde{\boldsymbol{\Phi}}^{-1}\\ &\quad\times\begin{pmatrix}\boldsymbol{\mathcal{A}}_M & \boldsymbol{0}_{LM\times KM}\\ \boldsymbol{0}_{LM\times KM} & \boldsymbol{\mathcal{A}}_M^*\end{pmatrix}\begin{pmatrix}\boldsymbol{C}_{li} & \boldsymbol{C}'_{li}\\ \boldsymbol{C}'_{li}{}^* & \boldsymbol{C}_{li}^*\end{pmatrix}\Bigg)\Bigg\}.\end{aligned}$$

The last expression is equivalent to

$$\begin{aligned}[\boldsymbol{H}]_{ik} &= 4\Re\left\{\left(\boldsymbol{d}_i^H\boldsymbol{C}^{-\frac{1}{2}}\boldsymbol{\Pi}_0^\perp\boldsymbol{C}^{-\frac{1}{2}}\boldsymbol{d}_k\right)\begin{pmatrix}C_{lk}^H & \boldsymbol{C}'_{lk}{}^T\end{pmatrix}\right.\\ &\left.\times\begin{pmatrix}\boldsymbol{\mathcal{A}}_M^H & \boldsymbol{0}_{KM\times LM}\\ \boldsymbol{0}_{KM\times LM} & \boldsymbol{\mathcal{A}}_M^T\end{pmatrix}\tilde{\boldsymbol{\Phi}}^{-1}\begin{pmatrix}\boldsymbol{\mathcal{A}}_M & \boldsymbol{0}_{LM\times KM}\\ \boldsymbol{0}_{LM\times KM} & \boldsymbol{\mathcal{A}}_M^*\end{pmatrix}\begin{pmatrix}\boldsymbol{C}_{li}\\ \boldsymbol{C}'_{li}{}^*\end{pmatrix}\right\}.\end{aligned}$$

Consequently, we obtain the expression of $\boldsymbol{H}$ as given by (48).

Appendix B
Derivation of $\boldsymbol{Q}$

We denote by $\boldsymbol{V}_i(\boldsymbol{\theta})$ the derivative of $\boldsymbol{V}(\boldsymbol{\theta})$ with respect to θ_i. Similarly to [11], $\boldsymbol{V}_i(\boldsymbol{\theta})$ has the following expression:

$$\boldsymbol{V}_i(\boldsymbol{\theta}) \simeq -2\Re\left\{\mathrm{tr}\left(\tilde{\boldsymbol{D}}_i^H\tilde{\boldsymbol{C}}^{-\frac{1}{2}}\tilde{\boldsymbol{\Pi}}_0^\perp\tilde{\boldsymbol{C}}^{-\frac{1}{2}}\tilde{\boldsymbol{X}}_N\tilde{\boldsymbol{\Phi}}^{-1}\tilde{\boldsymbol{\Sigma}}\tilde{\boldsymbol{A}}^{\dagger H}\right)\right\}$$

where

$$\tilde{\boldsymbol{X}}_N = \frac{1}{n-M}\sum_{t=\frac{M}{2}+1}^{n-\frac{M}{2}}\tilde{\boldsymbol{w}}(t)\tilde{\boldsymbol{\phi}}^H(t) = \begin{pmatrix}\boldsymbol{X}_N & \boldsymbol{X}'_N\\ \boldsymbol{X}'^*_N & \boldsymbol{X}^*_N\end{pmatrix}$$

with

$$\boldsymbol{X}_N = \frac{1}{n-M}\sum_{t=\frac{M}{2}+1}^{n-\frac{M}{2}}\boldsymbol{w}(t)\boldsymbol{\phi}^H(t)$$
$$\boldsymbol{X}'_N = \frac{1}{n-M}\sum_{t=\frac{M}{2}+1}^{n-\frac{M}{2}}\boldsymbol{w}(t)\boldsymbol{\phi}^T(t).$$

After some algebraic manipulations, $\boldsymbol{V}_i(\boldsymbol{\theta})$ can be obtained as

$$\begin{aligned}\boldsymbol{V}_i(\boldsymbol{\theta}) \simeq -4\Re\Bigg\{&\left(\boldsymbol{d}_i^H\boldsymbol{C}^{-\frac{1}{2}}\boldsymbol{\Pi}_0^\perp\boldsymbol{C}^{-\frac{1}{2}}\boldsymbol{X}_N\boldsymbol{h}_i\right.\\ &\left.+\boldsymbol{d}_i^H\boldsymbol{C}^{-\frac{1}{2}}\boldsymbol{\Pi}_0^\perp\boldsymbol{C}^{-\frac{1}{2}}\boldsymbol{X}'_N\boldsymbol{g}_i\right)\Bigg\}\end{aligned}\quad(62)$$

where $\boldsymbol{h}_i$ and $\boldsymbol{g}_i$ are the i^{th} columns of the block matrices

$$\left(\tilde{\boldsymbol{\Phi}}^{-1}\tilde{\boldsymbol{\Sigma}}\tilde{\boldsymbol{A}}^{\dagger H}\right)_{(1:ML,1:K)}$$

and

$$\left(\tilde{\boldsymbol{\Phi}}^{-1}\tilde{\boldsymbol{\Sigma}}\tilde{\boldsymbol{A}}^{\dagger H}\right)_{(1:ML,K+1:2K)}$$

respectively. We also introduce $\boldsymbol{\alpha}_i$ as the i^{th} column of the matrix $\boldsymbol{C}^{-\frac{1}{2}}\boldsymbol{\Pi}_0^\perp\boldsymbol{C}^{-\frac{1}{2}}\boldsymbol{D}$. Then, (62) becomes

$$\boldsymbol{V}_i(\boldsymbol{\theta}) \simeq -4\Re\left\{\left(\boldsymbol{\alpha}_i^H\boldsymbol{X}_N\boldsymbol{h}_i + \boldsymbol{\alpha}_i^H\boldsymbol{X}'_N\boldsymbol{g}_i\right)\right\}.\quad(63)$$

Moreover, we have for two arbitrary scalars x and y, $\Re\{x\}\Re\{y\} = \frac{1}{2}\Re\{x^Hy + xy\}$. Applying this relation to (63) yields

$$\begin{aligned}&\mathrm{E}\{\boldsymbol{V}_i(\boldsymbol{\theta})\boldsymbol{V}_j(\boldsymbol{\theta})\} = 8\times\\ &\Big(\Re\left\{\mathrm{E}\left\{\boldsymbol{h}_i^H\boldsymbol{X}_N^H\boldsymbol{\alpha}_i\boldsymbol{\alpha}_j^H\boldsymbol{X}_N\boldsymbol{h}_j + \boldsymbol{\alpha}_i^H\boldsymbol{X}_N\boldsymbol{h}_i\boldsymbol{\alpha}_j^H\boldsymbol{X}_N\boldsymbol{h}_j\right\}\right\}\\ &+\Re\left\{\mathrm{E}\left\{\boldsymbol{g}_i^H\boldsymbol{X}_N'^H\boldsymbol{\alpha}_i\boldsymbol{\alpha}_j^H\boldsymbol{X}'_N\boldsymbol{g}_j + \boldsymbol{\alpha}_i^H\boldsymbol{X}'_N\boldsymbol{g}_i\boldsymbol{\alpha}_j^H\boldsymbol{X}'_N\boldsymbol{g}_j\right\}\right\}\\ &+\Re\left\{\mathrm{E}\left\{\boldsymbol{h}_i^H\boldsymbol{X}_N^H\boldsymbol{\alpha}_i\boldsymbol{\alpha}_j^H\boldsymbol{X}'_N\boldsymbol{g}_j + \boldsymbol{\alpha}_i^H\boldsymbol{X}_N\boldsymbol{h}_i\boldsymbol{\alpha}_j^H\boldsymbol{X}'_N\boldsymbol{g}_j\right\}\right\}\\ &+\Re\left\{\mathrm{E}\left\{\boldsymbol{g}_i^H\boldsymbol{X}_N'^H\boldsymbol{\alpha}_i\boldsymbol{\alpha}_j^H\boldsymbol{X}_N\boldsymbol{h}_j + \boldsymbol{\alpha}_i^H\boldsymbol{X}'_N\boldsymbol{g}_i\boldsymbol{\alpha}_j^H\boldsymbol{X}_N\boldsymbol{h}_j\right\}\right\}\Big)\\ &+o\left(\frac{1}{N}\right).\end{aligned}\quad(64)$$

From [12], we have $\mathrm{E}\left\{\boldsymbol{X}_N^H\boldsymbol{\alpha}_i\boldsymbol{\alpha}_j^H\boldsymbol{X}_N\right\} = \frac{1}{N}\boldsymbol{\alpha}_j^H\boldsymbol{C}\boldsymbol{\alpha}_i\boldsymbol{\Phi}$. In the same way, we derive $\mathrm{E}\left\{\boldsymbol{X}_N'^H\boldsymbol{\alpha}_i\boldsymbol{\alpha}_j^H\boldsymbol{X}'_N\right\}$ as follows:

$$\begin{aligned}&\mathrm{E}\left\{\boldsymbol{X}_N'^H\boldsymbol{\alpha}_i\boldsymbol{\alpha}_j^H\boldsymbol{X}'_N\right\}\\ &\quad= \frac{1}{N^2}\sum_{t,s}\mathrm{E}\left\{\boldsymbol{\alpha}_j^H\boldsymbol{w}(s)\boldsymbol{w}^H(t)\boldsymbol{\alpha}_i\boldsymbol{\phi}^*(t)\boldsymbol{\phi}^T(s)\right\},\\ &\quad= \frac{1}{N}\boldsymbol{\alpha}_j^H\boldsymbol{C}\boldsymbol{\alpha}_i\boldsymbol{\Phi}^*.\end{aligned}$$

Moreover, we obtain the expressions of $\mathrm{E}\left\{\boldsymbol{X}_N^H\boldsymbol{\alpha}_i\boldsymbol{\alpha}_j^H\boldsymbol{X}'_N\right\}$ and $\mathrm{E}\left\{\boldsymbol{X}_N'^H\boldsymbol{\alpha}_i\boldsymbol{\alpha}_j^H\boldsymbol{X}_N\right\}$, respectively, as

$$\begin{aligned}&\mathrm{E}\left\{\boldsymbol{X}_N^H\boldsymbol{\alpha}_i\boldsymbol{\alpha}_j^H\boldsymbol{X}'_N\right\}\\ &\quad= \frac{1}{N^2}\sum_{t,s}\mathrm{E}\left\{\boldsymbol{\alpha}_j^H\boldsymbol{w}(s)\boldsymbol{w}^H(t)\boldsymbol{\alpha}_i\boldsymbol{\phi}(t)\boldsymbol{\phi}^T(s)\right\}\\ &\quad= \frac{1}{N}\boldsymbol{\alpha}_j^H\boldsymbol{C}\boldsymbol{\alpha}_i\boldsymbol{\Phi}'\\ &\mathrm{E}\left\{\boldsymbol{X}_N'^H\boldsymbol{\alpha}_i\boldsymbol{\alpha}_j^H\boldsymbol{X}_N\right\}\\ &\quad= \frac{1}{N^2}\sum_{t,s}\mathrm{E}\left\{\boldsymbol{\alpha}_j^H\boldsymbol{w}(s)\boldsymbol{w}^H(t)\boldsymbol{\alpha}_i\boldsymbol{\phi}^*(t)\boldsymbol{\phi}^H(s)\right\}\\ &\quad= \frac{1}{N}\boldsymbol{\alpha}_j^H\boldsymbol{C}\boldsymbol{\alpha}_i\boldsymbol{\Phi}'^*.\end{aligned}$$

On the other hand, to derive $\mathrm{E}\left\{\boldsymbol{\alpha}_i^H\boldsymbol{X}_N\boldsymbol{h}_i\boldsymbol{\alpha}_j^H\boldsymbol{X}_N\boldsymbol{h}_j\right\}$, we consider the fact that $\boldsymbol{\alpha}_i^H\boldsymbol{X}_N\boldsymbol{h}_i$ is scalar. Therefore, we have

$$\mathrm{E}\left\{\boldsymbol{\alpha}_i^H\boldsymbol{X}_N\boldsymbol{h}_i\boldsymbol{\alpha}_j^H\boldsymbol{X}_N\boldsymbol{h}_j\right\} = \mathrm{E}\left\{\boldsymbol{h}_i^T\boldsymbol{X}_N^T\boldsymbol{\alpha}_i^*\boldsymbol{\alpha}_j^H\boldsymbol{X}_N\boldsymbol{h}_j\right\}.\quad(65)$$

Since the noise $\boldsymbol{w}(t)$ is circularly symmetric, then we conclude easily from (65) that

$$\mathrm{E}\left\{\boldsymbol{\alpha}_i^H \boldsymbol{X}_N \boldsymbol{h}_i \boldsymbol{\alpha}_j^H \boldsymbol{X}_N \boldsymbol{h}_j\right\} = 0.$$

In the same way, we prove that

$$\begin{aligned}\mathrm{E}\left\{\boldsymbol{\alpha}_i^H \boldsymbol{X}'_N \boldsymbol{g}_i \boldsymbol{\alpha}_j^H \boldsymbol{X}'_N \boldsymbol{g}_j\right\} &= \mathrm{E}\left\{\boldsymbol{\alpha}_i^H \boldsymbol{X}_N \boldsymbol{h}_i \boldsymbol{\alpha}_j^H \boldsymbol{X}'_N \boldsymbol{g}_j\right\} \\ &= \mathrm{E}\left\{\boldsymbol{\alpha}_i^H \boldsymbol{X}'_N \boldsymbol{g}_i \boldsymbol{\alpha}_j^H \boldsymbol{X}_N \boldsymbol{h}_j\right\} \\ &= 0.\end{aligned}$$

Therefore, we obtain, from (64), the following expression of $\mathrm{E}\left\{\boldsymbol{V}_i(\boldsymbol{\theta})\boldsymbol{V}_j(\boldsymbol{\theta})\right\}$:

$$\begin{aligned}\mathrm{E}\left\{\boldsymbol{V}_i(\boldsymbol{\theta})\boldsymbol{V}_j(\boldsymbol{\theta})\right\} = \frac{8}{N}\Re\Big\{\left(\boldsymbol{\alpha}_i^H \boldsymbol{C}\boldsymbol{\alpha}_j\right)\Big(\boldsymbol{h}_j^H \boldsymbol{\Phi}\boldsymbol{h}_i \\ + \boldsymbol{g}_j^H \boldsymbol{\Phi}^* \boldsymbol{g}_i + \boldsymbol{g}_j^H \boldsymbol{\Phi}'^* \boldsymbol{h}_i + \boldsymbol{h}_j^H \boldsymbol{\Phi}' \boldsymbol{g}_i\Big)\Big\} + o\left(\frac{1}{N}\right).\end{aligned}$$

This expression is equivalent to

$$\begin{aligned}&\mathrm{E}\left\{\boldsymbol{V}_i(\boldsymbol{\theta})\boldsymbol{V}_j(\boldsymbol{\theta})\right\} \\ &\quad= \frac{8}{N}\Re\left\{\left(\boldsymbol{\alpha}_i^H \boldsymbol{C}\boldsymbol{\alpha}_j\right)\left(\boldsymbol{h}_j^H \boldsymbol{g}_j^H\right)\tilde{\boldsymbol{\Phi}}\begin{pmatrix}\boldsymbol{h}_i \\ \boldsymbol{g}_i\end{pmatrix}\right\} + o\left(\frac{1}{N}\right). \quad (66)\end{aligned}$$

Now, we have

$$\begin{aligned}&\left(\boldsymbol{C}^{-\frac{1}{2}}\boldsymbol{\Pi}_0^{\perp}\boldsymbol{C}^{-\frac{1}{2}}\boldsymbol{D}\right)^H \boldsymbol{C}\left(\boldsymbol{C}^{-\frac{1}{2}}\boldsymbol{\Pi}_0^{\perp}\boldsymbol{C}^{-\frac{1}{2}}\boldsymbol{D}\right) \\ &\qquad= \boldsymbol{D}^H \boldsymbol{C}^{-\frac{1}{2}}\boldsymbol{\Pi}_0^{\perp}\boldsymbol{C}^{-\frac{1}{2}}\boldsymbol{D}. \quad (67)\end{aligned}$$

We also have

$$\begin{aligned}&\left(\tilde{\boldsymbol{\Phi}}^{-1}\tilde{\boldsymbol{\Sigma}}\tilde{\boldsymbol{A}}^{\dagger H}\right)^H \tilde{\boldsymbol{\Phi}}\left(\tilde{\boldsymbol{\Phi}}^{-1}\tilde{\boldsymbol{\Sigma}}\tilde{\boldsymbol{A}}^{\dagger H}\right) = \tilde{\boldsymbol{A}}^{\dagger}\tilde{\boldsymbol{\Sigma}}^H\tilde{\boldsymbol{\Phi}}^{-1}\tilde{\boldsymbol{\Sigma}}\tilde{\boldsymbol{A}}^{\dagger H}, \\ &= \begin{pmatrix}\boldsymbol{A}^{\dagger}\boldsymbol{\Sigma}^H & \boldsymbol{A}^{\dagger}\boldsymbol{\Sigma}'^T \\ \boldsymbol{A}^{\dagger *}\boldsymbol{\Sigma}'^H & \boldsymbol{A}^{\dagger *}\boldsymbol{\Sigma}^T\end{pmatrix}\tilde{\boldsymbol{\Phi}}^{-1}\begin{pmatrix}\boldsymbol{\Sigma}\boldsymbol{A}^{\dagger H} & \boldsymbol{\Sigma}'\boldsymbol{A}^{\dagger T} \\ \boldsymbol{\Sigma}'^*\boldsymbol{A}^{\dagger H} & \boldsymbol{\Sigma}^*\boldsymbol{A}^{\dagger T}\end{pmatrix}. \quad (68)\end{aligned}$$

Consequently, from (47), (66)–(68), we conclude that

$$\begin{aligned}\boldsymbol{Q} = 8\Re\Bigg\{&\left(\boldsymbol{D}^H\boldsymbol{C}^{-\frac{1}{2}}\boldsymbol{\Pi}_0{}^{\perp}\boldsymbol{C}^{-\frac{1}{2}}\boldsymbol{D}\right) \\ &\odot\left(\begin{pmatrix}\boldsymbol{A}^{\dagger}\boldsymbol{\Sigma}^H & \boldsymbol{A}^{\dagger}\boldsymbol{\Sigma}'^T\end{pmatrix}\tilde{\boldsymbol{\Phi}}^{-1}\begin{pmatrix}\boldsymbol{\Sigma}\boldsymbol{A}^{\dagger H} \\ \boldsymbol{\Sigma}'^*\boldsymbol{A}^{\dagger H}\end{pmatrix}\right)^T\Bigg\}.\end{aligned}$$

Using (22) and (23) and some algebraic manipulations yield the expression of $\boldsymbol{Q}$ as given by (49).

Appendix C
Proof of (55)

We have

$$\left[\mathrm{CRB}^{-1}(\boldsymbol{\theta})\right]_{ik} = \Re\left\{\mathrm{tr}\left(\tilde{\bar{\boldsymbol{G}}}_i^H \boldsymbol{\Pi}_{\tilde{\bar{\boldsymbol{G}}}}^{\perp}\tilde{\bar{\boldsymbol{G}}}_k\tilde{\boldsymbol{\mathcal{P}}}\tilde{\bar{\boldsymbol{G}}}^H\tilde{\boldsymbol{\mathcal{R}}}_N^{-1}\tilde{\bar{\boldsymbol{G}}}\tilde{\boldsymbol{\mathcal{P}}}\right)\right\}.$$

This expression is equivalent to

$$\begin{aligned}\left(\mathrm{CRB}^{-1}(\boldsymbol{\theta})\right)_{ik} = \Re\Bigg\{&\mathrm{tr}\Bigg(\begin{pmatrix}\bar{\boldsymbol{G}}_i^H\boldsymbol{\Pi}_{\bar{\boldsymbol{G}}}^{\perp}\bar{\boldsymbol{G}}_k & \boldsymbol{0} \\ \boldsymbol{0} & \bar{\boldsymbol{G}}_i^T\boldsymbol{\Pi}_{\bar{\boldsymbol{G}}}^{\perp *}\bar{\boldsymbol{G}}_k^*\end{pmatrix} \\ &\times\begin{pmatrix}\boldsymbol{\mathcal{P}}\bar{\boldsymbol{G}}^H & \boldsymbol{\mathcal{P}}'\bar{\boldsymbol{G}}^T \\ \boldsymbol{\mathcal{P}}'^*\bar{\boldsymbol{G}}^H & \boldsymbol{\mathcal{P}}^*\bar{\boldsymbol{G}}^T\end{pmatrix}\tilde{\boldsymbol{\mathcal{R}}}_N^{-1}\begin{pmatrix}\bar{\boldsymbol{G}}\boldsymbol{\mathcal{P}} & \bar{\boldsymbol{G}}\boldsymbol{\mathcal{P}}' \\ \bar{\boldsymbol{G}}^*\boldsymbol{\mathcal{P}}'^* & \bar{\boldsymbol{G}}^*\boldsymbol{\mathcal{P}}^*\end{pmatrix}\Bigg)\Bigg\}. \quad (69)\end{aligned}$$

Observing that $\boldsymbol{\Pi}_{\bar{\boldsymbol{G}}}^{\perp} = \boldsymbol{I}_N \otimes \boldsymbol{\Pi}_{\bar{\boldsymbol{G}}}^{\perp}$, we obtain

$$\begin{aligned}\left[\mathrm{CRB}^{-1}(\boldsymbol{\theta})\right]_{ik} = 2\Re\Bigg\{&\mathrm{tr}\Bigg(\left(\boldsymbol{I}_N \otimes \boldsymbol{A}_i^H\boldsymbol{C}^{-\frac{1}{2}}\boldsymbol{\Pi}_{\bar{\boldsymbol{G}}}^{\perp}\boldsymbol{C}^{-\frac{1}{2}}\boldsymbol{A}_k\right) \\ &\times\begin{pmatrix}\boldsymbol{\mathcal{P}}\bar{\boldsymbol{G}}^H & \boldsymbol{\mathcal{P}}'\bar{\boldsymbol{G}}^T\end{pmatrix}\tilde{\boldsymbol{\mathcal{R}}}_N^{-1}\begin{pmatrix}\bar{\boldsymbol{G}}\boldsymbol{\mathcal{P}} \\ \bar{\boldsymbol{G}}^*\boldsymbol{\mathcal{P}}'^*\end{pmatrix}\Bigg)\Bigg\}.\end{aligned}$$

Therefore, $\left[\mathrm{CRB}^{-1}(\boldsymbol{\theta})\right]_{ik}$ can be written as

$$\left[\mathrm{CRB}^{-1}(\boldsymbol{\theta})\right]_{ik} = 2\Re\left\{\sum_{j=1}^{N}\left(\boldsymbol{d}_i^H\boldsymbol{C}^{-\frac{1}{2}}\boldsymbol{\Pi}_{\bar{\boldsymbol{G}}}^{\perp}\boldsymbol{C}^{-\frac{1}{2}}\boldsymbol{d}_k\right)\{\boldsymbol{F}_j\}_{ki}\right\}$$

where $\boldsymbol{F}_j$ represents the $j^{\mathrm{th}}(K\times K)$ block on the diagonal of the matrix $\begin{pmatrix}\boldsymbol{\mathcal{P}}\bar{\boldsymbol{G}}^H & \boldsymbol{\mathcal{P}}'\bar{\boldsymbol{G}}^T\end{pmatrix}\tilde{\boldsymbol{\mathcal{R}}}_N^{-1}\begin{pmatrix}\bar{\boldsymbol{G}}\boldsymbol{\mathcal{P}} \\ \bar{\boldsymbol{G}}^*\boldsymbol{\mathcal{P}}'^*\end{pmatrix}$. Consequently, we obtain the following expression of $\mathrm{CRB}^{-1}(\boldsymbol{\theta})$:

$$\mathrm{CRB}^{-1}(\boldsymbol{\theta}) = 2\Re\left\{\sum_{j=1}^{N}\left(\boldsymbol{D}^H\boldsymbol{C}^{-\frac{1}{2}}\boldsymbol{\Pi}_{\bar{\boldsymbol{G}}}^{\perp}\boldsymbol{C}^{-\frac{1}{2}}\boldsymbol{D}\right)\odot\boldsymbol{F}_j^T\right\}.$$

We use the following identity:

$$\tilde{\boldsymbol{\mathcal{R}}}_N = \tilde{\boldsymbol{\mathcal{C}}}^{-\frac{1}{2}}\tilde{\boldsymbol{\mathcal{R}}}\tilde{\boldsymbol{\mathcal{C}}}^{-\frac{1}{2}}$$

where

$$\tilde{\boldsymbol{\mathcal{R}}} = \begin{pmatrix}\boldsymbol{\mathcal{R}} & \boldsymbol{\mathcal{R}}' \\ \boldsymbol{\mathcal{R}}'^* & \boldsymbol{\mathcal{R}}^*\end{pmatrix}$$

where $\boldsymbol{\mathcal{R}}$ and $\boldsymbol{\mathcal{R}}'$ are previously defined in (9) and (10), respectively. Then, after some algebraic manipulations, we obtain the expression of $\mathrm{CRB}^{\frac{\mathrm{cor}}{\mathrm{noncir}}}(\boldsymbol{\theta})$ as given by (55).

References

[1] P. Stoica and A. Nehorai, "Performance study of conditional and unconditional direction-of-Arrival estimation," *IEEE Trans. Acoust., Speech, Signal Process.*, vol. 38, pp. 1783–1795, Oct. 1990.

[2] P. Stoica and A. Nehorai, "MUSIC, maximum likelihood and Cramer-Rao bound," *IEEE Trans. Acoust., Speech, Signal Process.*, vol. 37, pp. 720–741, May 1989.

[3] P. Stoica and A. Nehorai, "MUSIC, maximum likelihood and Cramér-Rao bound: Further results and comparisons," *IEEE Trans. Acoust., Speech, Signal Process.*, vol. 38, pp. 2140–2150, Dec. 1990.

[4] R. Roy, T. Kailath, and A. B. Gershman, "ESPRIT, estimation of signal parameters via rotational invariance techniques," *IEEE Trans. Acoust., Speech, Signal Process.*, vol. 37, pp. 984–995, Jul. 1989.

[5] P. Stoica and K. C. Sharman, "Maximum likelihood methods for direction-of-Arrival estimation," *IEEE Trans. Acoust., Speech, Signal Process.*, vol. 38, pp. 1132–1143, Jul. 1990.

[6] M. Viberg and B. Ottersten, "Sensor array processing based on subspace fitting," *IEEE Trans. Signal Process.*, vol. 39, pp. 1110–1121, May 1991.

[7] B. Ottersten, M. Viberg, and T. Kailath, "Analysis of subspace fitting and ML techniques for parameter estimation from sensor array data," *IEEE Trans. Signal Process.*, vol. 40, pp. 590–600, Mar. 1992.

[8] J. Li, B. Halder, P. Stoica, and M. Viberg, "Computationally efficient angle estimation for signals with known waveforms," *IEEE Trans. Signal Process.*, vol. 43, pp. 2154–2163, Sep. 1995.

[9] M. Viberg, P. Stoica, and B. Ottersten, "Maximum likelihood array processing in spatially correlated noise fields using parameterized signals," *IEEE Trans. Signal Process.*, vol. 45, pp. 996–1004, Apr. 1997.

[10] M. Agrawal and S. Prasad, "A modified likelihood function approach to DOA estimation in the presence of unknown spatially correlated Gaussian noise using a uniform linear array," *IEEE Trans. Signal Process.*, vol. 48, no. 10, pp. 2743–2749, Oct. 2000.

[11] M. Pesavento and A. B. Gershman, "Maximum-likelihood direction-of-Arrival estimation in the presence of unknown nonuniform noise," *IEEE Trans. Signal Process.*, vol. 49, no. 7, pp. 1310–1324, Jul. 2001.

[12] P. Stoica, M. Viberg, and B. Ottersten, "Instrumental variable approach to array processing in spatially correlated noise fields," *IEEE Trans. Signal Process.*, vol. 42, pp. 121–133, Jan. 1994.
[13] M. Viberg, P. Stoica, and B. Ottersten, "Array processing in correlated noise fields based on instrumental variables and subspace fitting," *IEEE Trans. Signal Process.*, vol. 43, pp. 1187–1199, May 1995.
[14] J. P. Delmas, "Asymptotically minimum variance second-order estimation for noncircular signals with application to DOA estimation," *IEEE Trans. Signal Process.*, vol. 52, no. 5, pp. 1235–1241, May 2004.
[15] H. Abeida and J. P. Delmas, "MUSIC-like estimation of direction of arrival for noncircular sources," *IEEE Trans. Signal Process.*, vol. 54, no. 7, pp. 2678–2689, Jul. 2006.
[16] F. Haddadi, M. M. Nayebi, and M. R. Aref, "Direction-of-Arrival estimation for temporally correlated narrowband signals," *IEEE Trans. Signal Process.*, vol. 57, no. 4, pp. 600–609, Apr. 2009.
[17] P. Stoica and R. Moses, *Introduction to Spectral Analysis*. Upper Saddle River, NJ: Prentice-Hall, 1997.
[18] J. P. Delmas and H. Abeida, "Stochastic Cramér-Rao bound for noncircular signals with application to DOA estimation," *IEEE Trans. Signal Process.*, vol. 52, no. 11, pp. 3192–3199, Nov. 2004.
[19] P. Stoica, E. G. Larsson, and A. B. Gershman, "The stochastic CRB for array processing: A textbook derivation," *IEEE Signal Process. Lett.*, vol. 8, pp. 148–150, May 2001.

Sonia Ben Hassen was born in Sfax, Tunisia, on January 29, 1986. She received the Diplôme d'Ingénieur in signals and systems (with Hons.) and the M.Sc. degree (with Hons.) in telecommunication, both from Tunisia Polytechnic School in 2009 and 2010, respectively. She is currently working towards the Ph.D. degree in telecommunication at Tunisia Polytechnic School.

Her research interests focus mainly on statistical signal processing and array processing with an emphasis on direction-of-arrival (DOA) estimation for wireless communications.

Faouzi Bellili was born in Sbeitla, Kasserine, Tunisia, on June 16, 1983. He received the Diplôme d'Ingénieur degree in signals and systems (with Hons.) from the Tunisia Polytechnic School in 2007 and the M.Sc. degree, with exceptional grade, at the Institut National de la Recherche Scientifique-Energie, Matériaux, et Télécommunications (INRS-EMT), Université du Québec, Montréal, QC, Canada, in 2009. He is currently working towards the Ph.D. degree at the INRS-EMT.

During his M.Sc. studies, he has authored/coauthored six international journal papers and more than ten international conference papers. His research focuses on statistical signal processing and array processing with an emphasis on parameters estimation for wireless communications.

Mr. Bellili was selected by the INRS as its candidate for the 2009–2010 competition of the very prestigious Vanier Canada Graduate Scholarships program. He also received the Academic Gold Medal of the Governor General of Canada for the year 2009–2010 and the Excellence Grant of the Director General of INRS for the year 2009–2010. He also received the award of the best M.Sc. thesis of INRS-EMT for the year 2009–2010 and twice—for both the M.Sc. and Ph.D. programs—the National Grant of Excellence from the Tunisian Government. He was also rewarded in 2011 the Merit Scholarship for Foreign Students from the Ministère de l'Éducation, du Loisir et du Sport (MELS) of Québec, Canada. He serves regularly as a reviewer for many international scientific journals and conferences.

Abdelaziz Samet (M'09) was born in 1959. He received the B.Sc. degree in electrical engineering from the Ecole Nationale Supérieure de l'Electronique et de ses Applications (ENSEA), Cergy, France, in 1984 and the M.Sc. and Ph.D. degrees in electrical engineering from The Ecole Nationale d'Ingénieurs de Tunis (ENIT), Tunis, Tunisia, in 1988 and 1993, respectively.

He is currently a Professor at the Institut National des Sciences Appliquées et de Technologie (INSAT) and the Head of the Research Unit Electronic Systems and Components at the Ecole Polytechnique de Tunisie (EPT), Tunis, Tunisia. His current research interests include wireless communications and signal processing.

Sofiène Affes (S'94–M'95–SM'04) received the Diplôme d'Ingénieur degree in electrical engineering and the Ph.D. degree (with Hons.) in signal processing, both from the Ecole Nationale Supérieure des Télécommunications (ENST), Paris, France, in 1992 and 1995, respectively.

He has been since with INRS-EMT, University of Quebec, Montreal, QC, Canada, as a Research Associate from 1995 until 1997, as an Assistant Professor until 2000, and then as an Associate Professor until 2009. Currently, he is a Full Professor in the Wireless Communications Group. His research interests are in wireless communications, statistical signal and array processing, adaptive space-time processing, and MIMO. From 1998 to 2002, he has been leading the radio design and signal processing activities of the Bell/Nortel/NSERC Industrial Research Chair in Personal Communications at INRS-EMT, Montreal, QC, Canada. Since 2004, he has been actively involved in major projects in wireless communication of PROMPT (Partnerships for Research on Microelectronics, Photonics and Telecommunications).

Prof. Affes was the corecipient of the 2002 Prize for Research Excellence of INRS. He currently holds a Canada Research Chair in Wireless Communications and a Discovery Accelerator Supplement Award from NSERC (Natural Sciences & Engineering Research Council of Canada). In 2006, he served as a General Co-Chair of the IEEE Vehicular Technology Conference (VTC) 2006-Fall conference, Montreal, QC, Canada. In 2008, he received from the IEEE Vehicular Technology Society the IEEE VTC Chair Recognition Award for exemplary contributions to the success of IEEE VTC. He currently acts as a member of the Editorial Board of the IEEE TRANSACTIONS ON SIGNAL PROCESSING, the IEEE TRANSACTIONS ON WIRELESS COMMUNICATIONS, and the Wiley *Journal on Wireless Communications and Mobile Computing*.